Eur. Phys. J. C (2018) 78:1
https://doi.org/10.1140/epjc/s10052-017-5488-z

THE EUROPEAN PHYSICAL JOURNAL C

Regular Article - Theoretical Physics

CP violation in leptonic rare B_s^0 decays as a probe of new physics

Robert Fleischer[1,2,a], **Daniela Galárraga Espinosa**[1,3], **Ruben Jaarsma**[1], **Gilberto Tetlalmatzi-Xolocotzi**[1]

[1] Nikhef, Science Park 105, 1098 XG Amsterdam, The Netherlands
[2] Department of Physics and Astronomy, Vrije Universiteit Amsterdam, 1081 HV Amsterdam, The Netherlands
[3] Physics Department, Université Paris-Sud, 91405 Orsay, France

Received: 20 November 2017 / Accepted: 19 December 2017 / Published online: 29 December 2017

Abstract The decay $B_s^0 \to \mu^+\mu^-$ is a key probe for the search of physics beyond the Standard Model. While the current measurements of the corresponding branching ratio agree with the Standard Model within the uncertainties, significant New-Physics effects may still be hiding in $B_s^0 \to \mu^+\mu^-$. In order to reveal them, the observable $\mathcal{A}_{\Delta\Gamma_s}^{\mu\mu}$, which is provided by the decay width difference $\Delta\Gamma_s$ of the B_s^0-meson system, plays a central role. We point out that a measurement of a CP-violating observable $\mathcal{S}_{\mu\mu}$, which is induced through interference between B_s^0–$\bar{B}_s^0$ mixing and $B_s \to \mu^+\mu^-$ decay processes, is essential to obtain the full picture, in particular to establish new scalar contributions and CP-violating phases. We illustrate these findings with future scenarios for the upgrade(s) of the LHC, exploiting also relations which emerge within an effective field theory description of the Standard Model, complemented with New Physics entering significantly beyond the electroweak scale.

1 Introduction

The decay $B_s^0 \to \mu^+\mu^-$ is one of the most interesting processes offered by Nature, allowing us to test the Standard Model (SM) and probe New Physics (NP). In the SM, this channel has no contributions at the tree level and shows a helicity suppression [1]. Consequently, the SM branching ratio is enormously suppressed, and only about three out of one billion B_s^0 mesons decay into the $\mu^+\mu^-$ final state. Another key feature of $B_s^0 \to \mu^+\mu^-$ is related to the impact of strong interactions. As gluons do not couple to the leptonic final state, only the B_s^0 decay constant f_{B_s} enters the theoretical description, which can be calculated by means of lattice QCD [2].

As NP effects may enhance the branching ratio of $B_s^0 \to \mu^+\mu^-$ significantly, experiments have searched for this channel for decades [3]. It has been a highlight of the results of the Large Hadron Collider (LHC) that $B_s^0 \to \mu^+\mu^-$ could eventually be observed by the CMS and LHCb collaborations and is now experimentally well established [4], with a measured branching ratio in the ballpark of the SM prediction. In addition to the branching ratio, $B_s^0 \to \mu^+\mu^-$ offers another observable, $\mathcal{A}_{\Delta\Gamma_s}^{\mu\mu}$, which is accessible thanks to the sizeable decay width difference $\Delta\Gamma_s$ of the mass eigenstates of the B_s^0-meson system [5]. This observable is theoretically clean and plays an important role in the search for NP effects [6–8]. A pioneering measurement of $\mathcal{A}_{\Delta\Gamma_s}^{\mu\mu}$ has recently been reported by the LHCb collaboration [9]. This analysis requires, in contrast to the measurement of the branching ratio, time information for untagged B_s data samples.

If also tagging information is available, a CP-violating observable $\mathcal{S}_{\mu\mu}$ can be measured which arises from the interference between B_s^0–$\bar{B}_s^0$ mixing and decay processes. Should it be possible to determine the helicity of the final-state muons, yet another CP asymmetry $\mathcal{C}_{\mu\mu}$ can be measured, as discussed in detail in Refs. [5,6]. It is not independent from $\mathcal{A}_{\Delta\Gamma_s}^{\mu\mu}$ and $\mathcal{S}_{\mu\mu}$, as the observables satisfy the following relation:

$$\left(\mathcal{A}_{\Delta\Gamma_s}^{\mu\mu}\right)^2 + \left(\mathcal{S}_{\mu\mu}\right)^2 + \left(\mathcal{C}_{\mu\mu}\right)^2 = 1\,. \tag{1}$$

In these observables, as in the case of $\mathcal{A}_{\Delta\Gamma_s}^{\mu\mu}$, the decay constant f_{B_s} cancels. Consequently, they are theoretically clean. Within the SM, the CP asymmetries vanish. However, in the presence of physics beyond the SM, we may in general encounter new sources of CP violation, generating non-vanishing CP asymmetries and affecting also the observable $\mathcal{A}_{\Delta\Gamma_s}^{\mu\mu}$.

In analyses of rare $B_{(s)}$ decays, it is usually – for simplicity – assumed that CP-violating NP phases vanish. Within specific models, such assumptions can be made, where an important example is given by scenarios with "Minimal Flavour Violation" [10]. However, we would rather like to learn from

[a] e-mail: robert.fleischer@nikhef.nl

experimental data whether new CP-violating phases enter the dynamics of the decay $B_s^0 \to \mu^+\mu^-$.

In this paper, we explore this question. Interestingly, we find that $\mathcal{S}_{\mu\mu}$ is an essential observable to reveal the nature of possible NP effects. The sign of the CP asymmetry $\mathcal{C}_{\mu\mu}$ would allow us to resolve certain ambiguities. We shall illustrate these findings with various examples, showing in particular how we may establish new (pseudo)-scalar contributions to $B_s^0 \to \mu^+\mu^-$ and further resolve their structure and dynamics. These considerations are completely general and can also be applied to the rare $B_s^0 \to \tau^+\tau^-$ and $B_s^0 \to e^+e^-$ decays [8].

The outline of this paper is as follows: in Sect. 2, we discuss the theoretical description of $B_s^0 \to \mu^+\mu^-$ and introduce the corresponding observables. In Sect. 3, we explore then the situation with general CP-violating NP contributions. Assuming relations between short-distance coefficients, which are motivated by considerations within effective field theory, we analyze the interplay between the $B_s^0 \to \mu^+\mu^-$ observables in Sect. 4. In Sect. 5, we shall address experimental aspects by discussing scenarios and illustrating their physics reach by making assumptions about the experimental precision. Finally, we summarize our key results and give a brief outlook in Sect. 6.

2 Theoretical description and observables

2.1 Decay amplitude

The theoretical framework to describe the decay $\bar{B}_s^0 \to \mu^+\mu^-$ is given by effective quantum field theory, which allows the calculation of a low-energy effective Hamiltonian of the following general structure [1,5,7]:

$$\begin{aligned}\mathcal{H}_{\rm eff} = -\frac{G_{\rm F}}{\sqrt{2}\pi} V_{ts}^* V_{tb} \alpha \big[& C_{10} O_{10} + C_S O_S + C_P O_P \\ & + C'_{10} O'_{10} + C'_S O'_S + C'_P O'_P \big]. \end{aligned} \tag{2}$$

Here $G_{\rm F}$ is Fermi's constant, $V_{ts}^* V_{tb}$ is a factor with elements of the Cabibbo–Kobayashi–Maskawa (CKM) matrix, and α denotes the QED fine structure constant. The Wilson coefficients $C_{10}^{(\prime)}$, $C_P^{(\prime)}$ and $C_S^{(\prime)}$ describe heavy degrees of freedom, which have been integrated out from appearing as explicit fields, and are associated with the four-fermion operators

$$\begin{aligned} O_{10} &= (\bar{s}\gamma_\mu P_L b)(\bar{\mu}\gamma^\mu\gamma_5\mu), & O'_{10} &= (\bar{s}\gamma_\mu P_R b)(\bar{\mu}\gamma^\mu\gamma_5\mu), \\ O_S &= m_b(\bar{s}P_R b)(\bar{\mu}\mu), & O'_S &= m_b(\bar{s}P_L b)(\bar{\mu}\mu), \\ O_P &= m_b(\bar{s}P_R b)(\bar{\mu}\gamma_5\mu), & O'_P &= m_b(\bar{s}P_L b)(\bar{\mu}\gamma_5\mu), \end{aligned} \tag{3}$$

with m_b denoting the b-quark mass, and

$$P_L \equiv \frac{1}{2}(1-\gamma_5), \quad P_R \equiv \frac{1}{2}(1+\gamma_5). \tag{4}$$

In general, the Wilson coefficients are different for $b \to s$ and $b \to d$ transitions, and depend on the flavour of the final-state leptons [8]. For simplicity, we do not give the corresponding labels explicitly in the following discussion. In the SM, we have only to deal with the O_{10} operator, having a real coefficient $C_{10}^{\rm SM}$.

Introducing the combinations of Wilson coefficients

$$P \equiv \frac{C_{10} - C'_{10}}{C_{10}^{\rm SM}} + \frac{M_{B_s}^2}{2m_\mu}\left(\frac{m_b}{m_b+m_s}\right)\left(\frac{C_P - C'_P}{C_{10}^{\rm SM}}\right) \equiv |P| e^{i\varphi_P}, \tag{5}$$

$$S \equiv \sqrt{1-\frac{4m_\mu^2}{M_{B_s}^2}}\,\frac{M_{B_s}^2}{2m_\mu}\left(\frac{m_b}{m_b+m_s}\right)\left(\frac{C_S - C'_S}{C_{10}^{\rm SM}}\right) \equiv |S| e^{i\varphi_S}, \tag{6}$$

where M_{B_s}, m_μ, m_b, m_s are the corresponding particle masses and φ_P, φ_S denote CP-violating phases, we obtain the following expression for the decay amplitude [5]:

$$A(\bar{B}_s^0 \to \mu_\lambda^+\mu_\lambda^-) \propto V_{ts}^* V_{tb} f_{B_s} M_{B_s} m_\mu C_{10}^{\rm SM} [\eta_\lambda P + S]. \tag{7}$$

Here $\lambda = {\rm L}, {\rm R}$ describes the helicity of the final-state leptons with $\eta_{\rm L} = +1$ and $\eta_{\rm R} = -1$.

In the SM, we have

$$P|_{\rm SM} = 1, \quad S|_{\rm SM} = 0, \tag{8}$$

and the relevant Wilson coefficient is given as [6]

$$C_{10}^{\rm SM} = -\eta_Y \sin^{-2}\theta_W Y_0(x_t) = -4.134, \tag{9}$$

where η_Y describes QCD corrections, θ_W is the weak mixing angle, $Y(x_t)$ represents one of the Inami–Lim functions, and $x_t \equiv m_t^2/M_W^2$ parametrizes the top-quark and W mass dependence [11]. We would like to emphasize that, by convention, $C_{10}^{\rm SM}$ does not have a complex phase. However, it takes a negative value, such that

$$C_{10}^{\rm SM} = -|C_{10}^{\rm SM}|. \tag{10}$$

In the following discussion, the CP-violating phases φ_P and φ_S play a central role. While the latter is directly related to the phase of the short-distance coefficient $C_S - C'_S$ of new scalar contributions, the former may get contributions both from $C_{10} - C'_{10}$ and from the coefficient $C_P - C'_P$, which arises from new pseudo-scalar operators.

2.2 Branching ratio and effective lifetime

Due to B_s^0–$\bar{B}_s^0$ mixing, an initially, i.e. at time $t = 0$, present B_s^0 meson evolves into a time-dependent linear combination of B_s^0 and $\bar{B}_s^0$ states. For the "untagged" rate

$$\begin{aligned}&\langle\Gamma(B_s(t)\to\mu^+_\lambda\mu^-_\lambda)\rangle\\&\equiv\Gamma(B^0_s(t)\to\mu^+_\lambda\mu^-_\lambda)+\Gamma(\bar{B}^0_s(t)\to\mu^+_\lambda\mu^-_\lambda)\\&\propto e^{-t/\tau_{B_s}}\left[\cosh(y_s t/\tau_{B_s})+\mathcal{A}^\lambda_{\Delta\Gamma_s}\sinh(y_s t/\tau_{B_s})\right]\\&=R^\lambda_{\rm H}e^{-\Gamma^{(s)}_{\rm H}t}+R^\lambda_{\rm L}e^{-\Gamma^{(s)}_{\rm L}t},\end{aligned}\tag{11}$$

no "tagging" of the initially present B_s meson is needed. This quantity depends only on two exponentials and involves the parameter

$$y_s\equiv\frac{\Delta\Gamma_s}{2\Gamma_s}=0.0645\pm0.0045,\tag{12}$$

which characterizes the decay width difference of the B_s mass eigenstates, with $\tau_{B_s}\equiv1/\Gamma_s$ denoting the B_s mean lifetime [12,13]; for the experimental value, see Ref. [14]. The decay dynamics enters through the following observable [5,6]:

$$\begin{aligned}\mathcal{A}^\lambda_{\Delta\Gamma_s}&=\frac{R^\lambda_{\rm H}-R^\lambda_{\rm L}}{R^\lambda_{\rm H}+R^\lambda_{\rm L}}\\&=\frac{|P|^2\cos(2\varphi_P-\phi^{\rm NP}_s)-|S|^2\cos(2\varphi_S-\phi^{\rm NP}_s)}{|P|^2+|S|^2}\\&\equiv\mathcal{A}^{\mu\mu}_{\Delta\Gamma_s},\end{aligned}\tag{13}$$

which is independent of the muon helicity, as reflected by the definition of $\mathcal{A}^{\mu\mu}_{\Delta\Gamma_s}$. Within the SM, we have

$$\mathcal{A}^{\mu\mu}_{\Delta\Gamma_s}|_{\rm SM}=+1.\tag{14}$$

The phase $\phi^{\rm NP}_s$ originates from possible CP-violating NP contributions to the B^0_s–$\bar{B}^0_s$ mixing phase

$$\phi_s=-2\beta_s+\phi^{\rm NP}_s,\tag{15}$$

which is already strongly constrained by experimental data for CP-violating effects in $B^0_s\to J/\psi\phi$ and decays with similar dynamics, yielding the following results [14–16]:

$$\phi_s=-0.030\pm0.033=-(1.72\pm1.89)^\circ\tag{16}$$

$$\phi^{\rm NP}_s=0.007\pm0.033=(0.4\pm1.9)^\circ,\tag{17}$$

where we have used the SM value $\phi^{\rm SM}_s=-2\beta_s=-(2.12\pm0.04)^\circ$ in Eq. (17).

Since it is challenging to measure the muon helicity, we consider the helicity-summed rates

$$\Gamma(B^0_s(t)\to\mu^+\mu^-)\equiv\sum_{\lambda={\rm L,R}}\Gamma(B^0_s(t)\to\mu^+_\lambda\mu^-_\lambda)\tag{18}$$

$$\Gamma(\bar{B}^0_s(t)\to\mu^+\mu^-)\equiv\sum_{\lambda={\rm L,R}}\Gamma(\bar{B}^0_s(t)\to\mu^+_\lambda\mu^-_\lambda),\tag{19}$$

and use them to define an untagged rate $\langle\Gamma(B_s(t)\to\ell^+\ell^-)\rangle$ in analogy to Eq. (11). The branching ratio reported by experiments actually corresponds to the following time-integrated untagged rate [5,12]:

$$\overline{\mathcal{B}}(B_s\to\ell^+\ell^-)\equiv\frac{1}{2}\int_0^\infty\langle\Gamma(B_s(t)\to\ell^+\ell^-)\rangle\,dt.\tag{20}$$

Combining the CMS result from 2013 [17] with the most recent LHCb analysis [9] yields

$$\overline{\mathcal{B}}(B_s\to\mu^+\mu^-)_{\rm LHCb'17+CMS}=(3.0\pm0.5)\times10^{-9}.\tag{21}$$

This average was calculated by means of the Particle Data Group (PDG) procedure [18]. For comparison, we give also the constraint $\overline{\mathcal{B}}(B_s\to\mu^+\mu^-)_{\rm ATLAS'16}=(0.9^{+1.1}_{-0.8})\times10^{-9}$ reported by the ATLAS collaboration [19].

In the SM, we have the following expression [1]:

$$\begin{aligned}\overline{\mathcal{B}}(B_s\to\mu^+\mu^-)_{\rm SM}=&\frac{\tau_{B_s}G_F^4M_W^4\sin^4\theta_W}{8\pi^5}\frac{\left|C^{\rm SM}_{10}V_{ts}V^*_{tb}\right|^2}{(1-y_s)}\\&\times f^2_{B_s}M_{B_s}m^2_\mu\sqrt{1-4\frac{m^2_\mu}{M^2_{B_s}}},\end{aligned}\tag{22}$$

where special care has to be taken concerning the use of renormalization schemes to properly include next-to-leading-order electroweak corrections (for details, see Ref. [1]). Using current state-of-the-art input parameters yields the following result [8]:

$$\overline{\mathcal{B}}(B_s\to\mu^+\mu^-)_{\rm SM}=(3.57\pm0.16)\times10^{-9}.\tag{23}$$

In a very recent analysis [20], QED corrections from dynamics below the renormalization scale $\mu=m_b$ were calculated, affecting the branching ratio by almost 1%.

In order to search for NP effects by means of the branching ratio of $B^0_s\to\mu^+\mu^-$, the following ratio plays the key role [5,6]:

$$\overline{R}\equiv\frac{\overline{\mathcal{B}}(B_s\to\mu^+\mu^-)}{\overline{\mathcal{B}}(B_s\to\mu^+\mu^-)_{\rm SM}},\tag{24}$$

taking by definition the SM value

$$\overline{R}|_{\rm SM}=1.\tag{25}$$

Using the expressions given above yields

$$\overline{R}=\left[\frac{1+\mathcal{A}^{\mu\mu}_{\Delta\Gamma_s}y_s}{1+y_s}\right](|P|^2+|S|^2)=\Upsilon_P|P|^2+\Upsilon_S|S|^2\tag{26}$$

with

$$\begin{aligned}\Upsilon_P&\equiv\left[\frac{1+y_s\cos(2\varphi_P-\phi^{\rm NP}_s)}{1+y_s}\right],\\\Upsilon_S&\equiv\left[\frac{1-y_s\cos(2\varphi_S-\phi^{\rm NP}_s)}{1+y_s}\right].\end{aligned}\tag{27}$$

The numerical results in Eqs. (21) and (23) give

$$\overline{R}\big|_{\text{LHCb'17+CMS}} = 0.84 \pm 0.16. \tag{28}$$

The effective lifetime of the decay $B_s^0 \to \mu^+\mu^-$, which is defined through

$$\tau^s_{\mu\mu} \equiv \frac{\int_0^\infty t\,\langle\Gamma(B_s(t) \to \mu^+\mu^-)\rangle\,dt}{\int_0^\infty \langle\Gamma(B_s(t) \to \mu^+\mu^-)\rangle\,dt}, \tag{29}$$

contains the same physics information as the observable $\mathcal{A}^{\mu\mu}_{\Delta\Gamma_s}$ [5]:

$$\mathcal{A}^{\mu\mu}_{\Delta\Gamma_s} = \frac{1}{y_s}\left[\frac{(1-y_s^2)\tau^s_{\mu\mu} - (1+y_s^2)\tau_{B_s}}{2\tau_{B_s} - (1-y_s^2)\tau^s_{\mu\mu}}\right]. \tag{30}$$

A pioneering measurement of the effective lifetime of $B_s^0 \to \mu^+\mu^-$ was recently reported by the LHCb collaboration [9]:

$$\tau^s_{\mu\mu} = \big[2.04 \pm 0.44(\text{stat}) \pm 0.05(\text{syst})\big]\,\text{ps}. \tag{31}$$

Using Eq. (30), this result can be converted into

$$\mathcal{A}^{\mu\mu}_{\Delta\Gamma_s} = 8.24 \pm 10.72, \tag{32}$$

where the error is fully dominated by the uncertainty of $\tau^s_{\mu\mu}$. In view of the general model-independent range

$$-1 \le \mathcal{A}^{\mu\mu}_{\Delta\Gamma_s} \le +1, \tag{33}$$

it will be crucial to improve the experimental precision for this observable at the LHC upgrade(s) in order to use this quantity for testing the flavour sector of the SM.

2.3 CP asymmetries

In contrast to the untagged B_s rate in Eq. (11), the tagged, time-dependent rates involve oscillatory $\sin(\Delta M_s t)$ and $\cos(\Delta M_s t)$ terms, where ΔM_s is the mass difference between the heavy and light B_s mass eigenstates. We obtain a CP-violating rate asymmetry of the following form [5,6]:

$$\frac{\Gamma(B_s^0(t) \to \mu^+_\lambda\mu^-_\lambda) - \Gamma(\bar{B}_s^0(t) \to \mu^+_\lambda\mu^-_\lambda)}{\Gamma(B_s^0(t) \to \mu^+_\lambda\mu^-_\lambda) + \Gamma(\bar{B}_s^0(t) \to \mu^+_\lambda\mu^-_\lambda)} = \frac{\mathcal{C}^\lambda_{\mu\mu}\cos(\Delta M_s t) + \mathcal{S}^\lambda_{\mu\mu}\sin(\Delta M_s t)}{\cosh(y_s t/\tau_{B_s}) + \mathcal{A}^\lambda_{\Delta\Gamma_s}\sinh(y_s t/\tau_{B_s})}, \tag{34}$$

with the observables

$$\mathcal{C}^\lambda_{\mu\mu} = -\eta_\lambda\left[\frac{2|PS|\cos(\varphi_P - \varphi_S)}{|P|^2 + |S|^2}\right] \equiv -\eta_\lambda\mathcal{C}_{\mu\mu} \xrightarrow{\text{SM}} 0, \tag{35}$$

$$\mathcal{S}^\lambda_{\mu\mu} = \frac{|P|^2\sin(2\varphi_P - \phi_s^{\text{NP}}) - |S|^2\sin(2\varphi_S - \phi_s^{\text{NP}})}{|P|^2 + |S|^2} \equiv \mathcal{S}_{\mu\mu} \xrightarrow{\text{SM}} 0, \tag{36}$$

where $\eta_{\text{L}} = +1$ and $\eta_{\text{R}} = -1$ for left- and right-handed muon helicity, respectively. It should be noted that the CP asymmetry $\mathcal{S}^\lambda_{\mu\mu}$, which is caused by interference between B_s^0–$\bar{B}_s^0$ mixing and $B_s \to \mu^+\mu^-$ decay processes, does actually not depend on the muon helicity, just as the observable $\mathcal{A}^{\mu\mu}_{\Delta\Gamma_s} \equiv \mathcal{A}^\lambda_{\Delta\Gamma_s}$. Using the helicity-summed rates introduced above yields

$$\frac{\Gamma(B_s^0(t) \to \mu^+\mu^-) - \Gamma(\bar{B}_s^0(t) \to \mu^+\mu^-)}{\Gamma(B_s^0(t) \to \mu^+\mu^-) + \Gamma(\bar{B}_s^0(t) \to \mu^+\mu^-)} = \frac{\mathcal{S}_{\mu\mu}\sin(\Delta M_s t)}{\cosh(y_s t/\tau_{B_s}) + \mathcal{A}^{\mu\mu}_{\Delta\Gamma_s}\sinh(y_s t/\tau_{B_s})}, \tag{37}$$

where the $\mathcal{C}^\lambda_{\mu\mu}$ terms cancel because of the η_λ factor. It should be noted that a non-vanishing $\mathcal{C}_{\mu\mu}$ would be a smoking-gun signal for a new scalar contribution S. CP-violating asymmetries of this kind in $B_{s,d} \to \ell^+\ell^-$ decays were also considered for various NP scenarios in Refs. [21–23], neglecting the effects of $\Delta\Gamma_s$ and the associated observable $\mathcal{A}^{\mu\mu}_{\Delta\Gamma_s}$. For a more recent study, including the untagged observable, see Ref. [6].

It should be stressed that the non-perturbative decay constant f_{B_s} cancels in $\mathcal{A}^{\mu\mu}_{\Delta\Gamma_s}$ as well as in $\mathcal{S}_{\mu\mu}$ and $\mathcal{C}_{\mu\mu}$, thereby making these observables theoretically clean probes for the search of NP signals [5,6]. In the SM, a tiny residual uncertainty arises from QED corrections, which lead to effects at the 10^{-5} and 10^{-3} levels for $\mathcal{A}^{\mu\mu}_{\Delta\Gamma_s}$ and the CP asymmetries $\mathcal{S}_{\mu\mu}$, $\mathcal{C}_{\mu\mu}$, respectively [20].

In the following discussion, we will explore the interplay of $\mathcal{A}^{\mu\mu}_{\Delta\Gamma_s}$ and $\mathcal{S}_{\mu\mu}$ with the observable $\overline{R}$ to search for NP and reveal its nature, in particular whether it involves new (pseudo)-scalar contributions. Experimental feasibility studies of measurements of the CP asymmetry in Eq. (37) have not yet been performed to the best of our knowledge. However, we envision that an effort should be made to perform such a measurement at the LHC upgrade(s). In view of the relation in Eq. (1), a measurement of $\mathcal{C}_{\mu\mu}$ would not provide independent information. As such an analysis would require the reconstruction of the muon helicity, it is much more challenging than the asymmetry in Eq. (37) involving the helicity-averaged rates. However, we will show that already information on just the sign of $\mathcal{C}_{\mu\mu}$ would be sufficient to resolve certain ambiguities affecting the determination of P and S. We encourage experimentalists to explore avenues to eventually measure the sign of the $\mathcal{C}_{\mu\mu}$ observable.

3 General CP-violating new physics

3.1 Theoretical description

Let us start the general discussion of the CP-violating coefficients P and S in Eqs. (5) and (6), respectively, with the ratio $\overline{R}$ in Eq. (24). Using the expression in Eq. (26), we obtain

$$r \equiv \left[\frac{1+y_s}{1+\mathcal{A}^{\mu\mu}_{\Delta\Gamma_s}\, y_s}\right]\overline{R} = |P|^2 + |S|^2. \tag{38}$$

If we had a precise measurement of $\mathcal{A}^{\mu\mu}_{\Delta\Gamma_s}$, we could straightforwardly convert $\overline{R}$ into r. In view of the large uncertainty in Eq. (32), we use the general range in Eq. (33) to calculate

$$0.69 \le r \le 1.13, \tag{39}$$

where we have also taken into account the 1σ uncertainty of $\overline{R}$, given in Eq. (28). This observable fixes a circular band with radius $\sqrt{r}$ in the $|P|$–$|S|$ plane, which we show in Fig. 1. Using the observable $\mathcal{A}^{\mu\mu}_{\Delta\Gamma_s}$, we can calculate a straight line in this plane through

$$\frac{|S|}{|P|} = \sqrt{\frac{\cos\Phi_P - \mathcal{A}^{\mu\mu}_{\Delta\Gamma_s}}{\cos\Phi_S + \mathcal{A}^{\mu\mu}_{\Delta\Gamma_s}}}, \tag{40}$$

where we have introduced the abbreviations

$$\Phi_P \equiv 2\varphi_P - \phi_s^{\rm NP}, \quad \Phi_S \equiv 2\varphi_S - \phi_s^{\rm NP}. \tag{41}$$

If we assume that the CP-violating phases φ_P and φ_S take trivial values, i.e. 0° or 180°, $\overline{R}$ allows us to fix a circle in the $|P|$–$|S|$ plane through Eq. (26), and the intersection with the straight line following from

$$\frac{|S|}{|P|} = \sqrt{\frac{\cos\phi_s^{\rm NP} - \mathcal{A}^{\mu\mu}_{\Delta\Gamma_s}}{\cos\phi_s^{\rm NP} + \mathcal{A}^{\mu\mu}_{\Delta\Gamma_s}}} = \sqrt{\frac{1-\mathcal{A}^{\mu\mu}_{\Delta\Gamma_s}}{1+\mathcal{A}^{\mu\mu}_{\Delta\Gamma_s}}} \tag{42}$$

fixes $|P|$ and $|S|$, as discussed in detail in Refs. [5–8]; note that we use the result for $\phi_s^{\rm NP}$ in Eq. (17). However, if we allow for general CP-violating phases, any point on the circle with radius $\sqrt{r}$ is allowed since we obtain $|S| = 0$ for $\cos\Phi_P = \mathcal{A}^{\mu\mu}_{\Delta\Gamma_s}$ and $|P| = 0$ for $\cos\Phi_S = -\mathcal{A}^{\mu\mu}_{\Delta\Gamma_s}$.

The measurement of a non-vanishing CP asymmetry $\mathcal{S}_{\mu\mu}$ would immediately establish the presence of non-trivial CP-violating phases. This observable fixes another straight line in the $|P|$–$|S|$ plane:

$$\frac{|S|}{|P|} = \sqrt{\frac{\sin\Phi_P - \mathcal{S}_{\mu\mu}}{\sin\Phi_S + \mathcal{S}_{\mu\mu}}}. \tag{43}$$

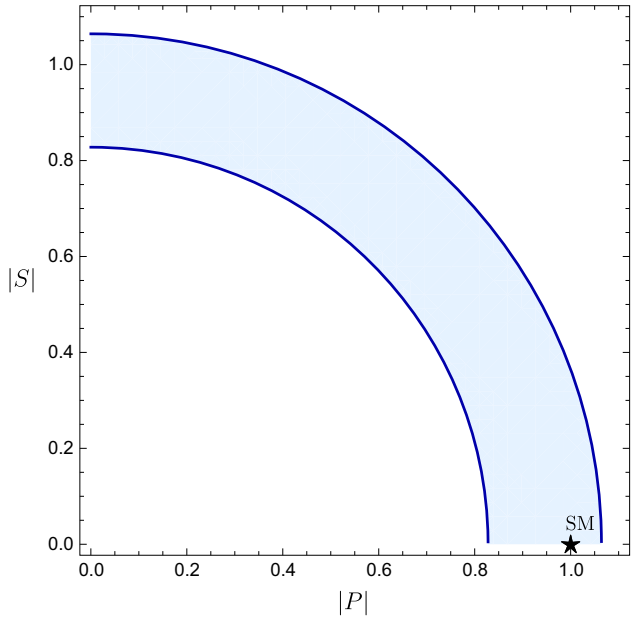

Fig. 1 Allowed region in the $|P|$–$|S|$ plane following from r, which is obtained by varying $\mathcal{A}^{\mu\mu}_{\Delta\Gamma_s}$ between -1 and $+1$ and taking the $1\,\sigma$ uncertainty of the current $\overline{R}$ measurement into account. The black star indicates the SM values given in Eq. (8)

However, as the CP-violating phases are in general unknown, the slope of this straight line is not determined, in analogy to the constraint following from $\mathcal{A}^{\mu\mu}_{\Delta\Gamma_s}$.

We have three independent observables at our disposal, r as well as $\mathcal{A}^{\mu\mu}_{\Delta\Gamma_s}$ and $\mathcal{S}_{\mu\mu}$, which depend on the four unknown parameters $|P|$, Φ_P and $|S|$, Φ_S. Using the general expressions for $\mathcal{A}^{\mu\mu}_{\Delta\Gamma_s}$ and $\mathcal{S}_{\mu\mu}$ in Eqs. (13) and (36), respectively, yields

$$A\cos\Phi_P - B\sin\Phi_P = C \tag{44}$$

with

$$A \equiv \mathcal{S}_{\mu\mu} + \sin\Phi_S \tag{45}$$

$$B \equiv \mathcal{A}^{\mu\mu}_{\Delta\Gamma_s} + \cos\Phi_S \tag{46}$$

$$C \equiv \mathcal{A}^{\mu\mu}_{\Delta\Gamma_s}\sin\Phi_S - \mathcal{S}_{\mu\mu}\cos\Phi_S. \tag{47}$$

This equation allows us to determine Φ_P as a function of Φ_S with the help of

$$\sin\Phi_P = -\left(\frac{BC}{A^2+B^2}\right) \pm \sqrt{\left(\frac{BC}{A^2+B^2}\right)^2 + \left(\frac{A^2-C^2}{A^2+B^2}\right)} \tag{48}$$

$$= \frac{-BC \pm |A|\sqrt{A^2+B^2-C^2}}{A^2+B^2}. \tag{49}$$

The expression under the square root is actually factorizable, thereby yielding

$$\sqrt{A^2+B^2-C^2} = \left|1 + \mathcal{A}^{\mu\mu}_{\Delta\Gamma_s}\cos\Phi_S + \mathcal{S}_{\mu\mu}\sin\Phi_S\right|. \tag{50}$$

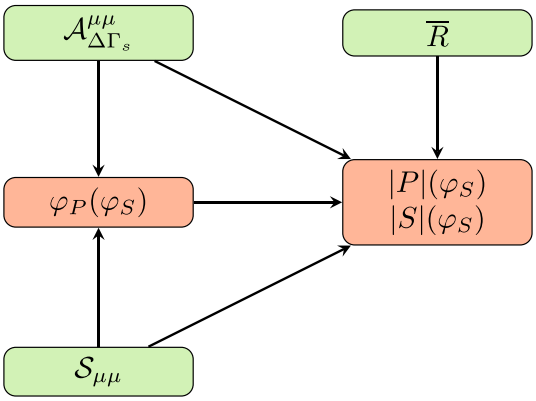

Fig. 2 Flowchart to illustrate the general strategy to determine $|P|$ and $|S|$ as functions of the the CP-violating phase φ_S from the $B_s^0 \to \mu^+\mu^-$ observables

Using then the observables r and $\mathcal{A}^{\mu\mu}_{\Delta\Gamma_s}$, we may determine

$$|P| = \sqrt{\left(\frac{\cos\Phi_S + \mathcal{A}^{\mu\mu}_{\Delta\Gamma_s}}{\cos\Phi_S + \cos\Phi_P}\right) r},$$
$$|S| = \sqrt{\left(\frac{\cos\Phi_P - \mathcal{A}^{\mu\mu}_{\Delta\Gamma_s}}{\cos\Phi_P + \cos\Phi_S}\right) r} \tag{51}$$

as functions of the CP-violating phase Φ_S. Using instead of $\mathcal{A}^{\mu\mu}_{\Delta\Gamma_s}$ the CP asymmetry $\mathcal{S}_{\mu\mu}$ yields

$$|P| = \sqrt{\left(\frac{\sin\Phi_S + \mathcal{S}_{\mu\mu}}{\sin\Phi_S + \sin\Phi_P}\right) r},$$
$$|S| = \sqrt{\left(\frac{\sin\Phi_P - \mathcal{S}_{\mu\mu}}{\sin\Phi_P + \sin\Phi_S}\right) r}. \tag{52}$$

The expression in Eq. (49) leaves us with a twofold ambiguity for φ_P for every value of φ_S. Information on the sign of $\mathcal{C}_{\mu\mu}$ allows us to determine the correct branch and thus obtain a single solution for φ_P as a function of φ_S. However, both branches have the same dependence of $|P|$ and $|S|$ on φ_S, so a single solution for $|P|$ and $|S|$ as a function of φ_S can be obtained even when no information on the sign of $\mathcal{C}_{\mu\mu}$ is available. In the flowchart in Fig. 2, we illustrate this general method for analyzing the observables provided by the $B_s^0 \to \mu^+\mu^-$ decay, and we will provide an example of this formalism in the next section.

3.2 Discussion and illustration

3.2.1 Vanishing mixing-induced CP violation

An interesting situation arises for $\mathcal{S}_{\mu\mu} = 0$. Although one may naively conclude that the CP-violating phases take then simply trivial values, this is actually not the case because of the structure of the expression in Eq. (36). In fact, we obtain the following extremal values on the circle with radius $\sqrt{r}$ in the $|P|$–$|S|$ plane:

$$|P_\pm| = \sqrt{\left(\frac{1 \mp \mathcal{A}^{\mu\mu}_{\Delta\Gamma_s}}{2}\right) r}, \quad |S_\pm| = \sqrt{\left(\frac{1 \pm \mathcal{A}^{\mu\mu}_{\Delta\Gamma_s}}{2}\right) r}, \tag{53}$$

where the region between these points can be accessed by varying Φ_S. In the case of $\mathcal{A}^{\mu\mu}_{\Delta\Gamma_s} = \pm 1$, we have

$$|S| = 0, \quad |P| = \sqrt{r}, \quad \sin\Phi_P = 0, \tag{54}$$

yielding $\mathcal{A}^{\mu\mu}_{\Delta\Gamma_s} = +\cos\Phi_P = \pm 1$, or

$$|P| = 0, \quad |S| = \sqrt{r}, \quad \sin\Phi_S = 0, \tag{55}$$

yielding $\mathcal{A}^{\mu\mu}_{\Delta\Gamma_s} = -\cos\Phi_S = \pm 1$. For $|\mathcal{A}^{\mu\mu}_{\Delta\Gamma_s}| < 1$, we get

$$\frac{|S|}{|P|} = \sqrt{\frac{(1 - \mathcal{A}^{\mu\mu}_{\Delta\Gamma_s})(1 + \mathcal{A}^{\mu\mu}_{\Delta\Gamma_s})}{1 + 2\,\mathcal{A}^{\mu\mu}_{\Delta\Gamma_s}\cos\Phi_S + (\mathcal{A}^{\mu\mu}_{\Delta\Gamma_s})^2}}. \tag{56}$$

A particularly interesting situation arises for $\mathcal{A}^{\mu\mu}_{\Delta\Gamma_s} = 0$, corresponding to the following point in the $|P|$–$|S|$ plane:

$$|P| = |S| = \sqrt{\frac{r}{2}}. \tag{57}$$

3.2.2 Sizeable mixing-induced CP violation

Let us now turn to mixing-induced CP violation in $B_s^0 \to \mu^+\mu^-$, and discuss a scenario with a large value of $\mathcal{S}_{\mu\mu}$, which requires significant CP-violating phases originating from physics beyond the SM. In order to illustrate this situation and the formalism discussed in Sect. 3.1, we consider an example which is characterized by

$$|S| = 0.30, \quad \varphi_S = 20^\circ. \tag{58}$$

Assuming furthermore

$$\varphi_P = 30^\circ, \tag{59}$$

the central value of the observable $\overline{R}$ in Eq. (28) yields

$$|P| = 0.89. \tag{60}$$

These values of $|P|$ and $|S|$ fall well within the currently allowed region in the $|P|$–$|S|$ plane shown in Fig. 1. We obtain the following set of observables:

$$\overline{R} = 0.84, \quad \mathcal{A}^{\mu\mu}_{\Delta\Gamma_s} = 0.37, \quad \mathcal{S}_{\mu\mu} = 0.71, \quad \mathcal{C}_{\mu\mu} = 0.60, \tag{61}$$

and assume that they were measured at a future experiment.

Let us now illustrate how we may obtain insights into NP effects using these observables. The deviation of $\mathcal{A}_{\Delta\Gamma_s}^{\mu\mu}$ from the SM prediction $+1$ would indicate NP effects. Having the measured $\mathcal{A}_{\Delta\Gamma_s}^{\mu\mu}$ at hand, we may use Eq. (38) to convert $\overline{R}$ into r, yielding

$$r = 0.87. \tag{62}$$

Moreover, the precision of the measured $B_s^0 \to \mu^+\mu^-$ branching ratio will then have significantly increased (see Sect. 5 for a more detailed discussion), allowing us to reduce the width of the circular band in Fig. 1. However, without any information on $\mathcal{S}_{\mu\mu}$, we could not narrow down further $|S|$ and $|P|$ in a model-independent way, i.e. we would still be left with the whole circular region, and could in particular not establish a non-vanishing scalar contribution S.

The measurement of the observable $\mathcal{S}_{\mu\mu}$ different from zero would signal new sources of CP violation. Using then Eq. (49), we could determine φ_P as a function of φ_S, as illustrated in Fig. 3. The information on the sign of $\mathcal{C}_{\mu\mu}$ would allow us to resolve the ambiguity, as indicated in the figure. Note that the points $(\varphi_S, \varphi_P) = (0°, 0°)$ and $(180°, 180°)$ would be excluded through the contours. Using Eqs. (51) or (52), we obtain $|S|$ and $|P|$ as functions of φ_S, as shown in Fig. 4. Here, information about the sign of $\mathcal{C}_{\mu\mu}$ plays no further role. Interestingly, we would now be able to put a lower bound on $|S|$, i.e. could conclude that we have new scalar contributions. We insist on the fact that in order to obtain this highly non-trivial information, a measurement of the CP asymmetry $\mathcal{S}_{\mu\mu}$ is required.

Although we can only determine the $B_s^0 \to \mu^+\mu^-$ parameters as functions of φ_S, this analysis would have profound implications, establishing in particular new scalar and pseudo-scalar contributions with CP-violating phases. In order to obtain further insights, more information is needed and assumptions about short-distance coefficients have to be made.

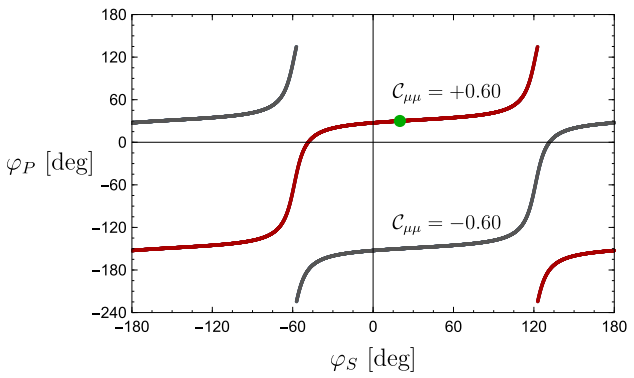

Fig. 3 Correlation between φ_P and φ_S for $\mathcal{A}_{\Delta\Gamma_s}^{\mu\mu} = 0.37$ and $\mathcal{S}_{\mu\mu} = 0.71$. The red and grey curves correspond to $\mathcal{C}_{\mu\mu} > 0$ and $\mathcal{C}_{\mu\mu} < 0$, respectively. The green dot marks the input parameters in Eq. (58)

4 Relations between (pseudo)-scalar coefficients

4.1 General framework

The effects of new particles enter the coefficients in Eqs. (5) and (6) through the short-distance coefficients C_P, C'_P and C_S, C'_S, which describe new pseudo-scalar and scalar contributions, respectively, and C_{10}, C'_{10}. As the constraints from the ATLAS and CMS experiments at the LHC for direct searches of new particles support the picture of a NP scale $\Lambda_{\rm NP}$ which is much larger than the electroweak scale $\Lambda_{\rm EW}$, the corresponding NP effects can be described in a model-independent way through an effective Lagrangian where the heavy degrees of freedom, i.e. the NP particles, have been integrated out at $\Lambda_{\rm NP}$. If we require then invariance under the SM gauge group $SU(2)_L \times U(1)_Y$ for the renormaliza-

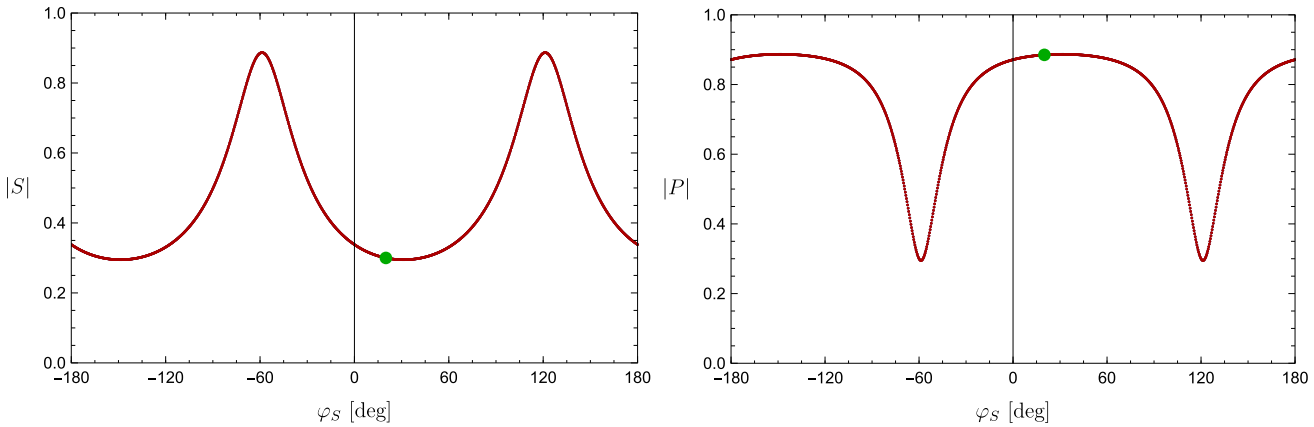

Fig. 4 The coefficients $|S|$ and $|P|$ determined as functions of φ_S for the example discussed in the text. The corresponding input parameters are marked by the green dot

tion group evolution between $\Lambda_{\rm NP}$ and $\Lambda_{\rm EW}$, a "SM Effective Field Theory" (SMEFT) can be set up [24,25] and matched to the effective Hamiltonian in Eq. (2) describing $B_s^0 \to \mu^+\mu^-$ decays. Following these lines and applying the machinery of effective quantum field theory, the following relations among the corresponding short-distance coefficients can be derived [26]:

$$C_P = -C_S \tag{63}$$
$$C'_P = C'_S. \tag{64}$$

A further application of these relations – assuming no new sources of CP violation – can be found in Ref. [7], while a fit of data to the SMEFT scenario with complex coefficients was performed in Ref. [27]. For a discussion within specific models, see Ref. [6].

In this section, we explore the implication of Eqs. (63) and (64) for the general analysis of CP violation discussed in Sect. 3. To this end, we express the relevant quantities in terms of the scalar short-distance coefficients

$$C_S \equiv |C_S| e^{i\tilde{\varphi}_S}, \quad C'_S \equiv |C'_S| e^{i\tilde{\varphi}'_S}, \tag{65}$$

which yields

$$\begin{aligned} P &\equiv |P| e^{i\varphi_P} = |P| \cos\varphi_P + i |P| \sin\varphi_P \\ &= \mathcal{C}_{10} - \frac{1}{w}\left[\frac{1+|x|e^{i\Delta}}{1-|x|e^{i\Delta}}\right] |S| e^{i\varphi_S} \end{aligned} \tag{66}$$

with

$$w \equiv \sqrt{1 - \frac{4m_\mu^2}{M_{B_s}^2}}, \quad \mathcal{C}_{10} \equiv \frac{C_{10} - C'_{10}}{C_{10}^{\rm SM}} \tag{67}$$

and

$$x \equiv |x| e^{i\Delta} \equiv \left|\frac{C'_S}{C_S}\right| e^{i(\tilde{\varphi}'_S - \tilde{\varphi}_S)}. \tag{68}$$

We will refer to this notation as the SMEFT parametrization. It it useful to write Eq. (66) in the following form:

$$w P + \left[\frac{1+|x|e^{i\Delta}}{1-|x|e^{i\Delta}}\right] S = w\, \mathcal{C}_{10}. \tag{69}$$

In the Appendix, we present expressions that allow us to obtain the $B_s^0 \to \mu^+\mu^-$ observables in terms of the parametrization introduced above. As P requires input for C_{10}, C'_{10}, we shall now first discuss these coefficients.

4.2 Closer look at C_{10} and C'_{10}

The Wilson coefficients C_{10} and C'_{10} enter in P through the following combination:

$$\mathcal{C}_{10} \equiv |\mathcal{C}_{10}| e^{i\varphi_{10}} \equiv \frac{C_{10} - C'_{10}}{C_{10}^{\rm SM}} = 1 + \mathcal{C}_{10}^{\rm NP}, \tag{70}$$

where φ_{10} is a CP-violating phase and

$$\mathcal{C}_{10}^{\rm NP} \equiv |\mathcal{C}_{10}^{\rm NP}| e^{i\varphi_{10}^{\rm NP}} = \frac{C_{10}^{\rm NP} - C'_{10}}{C_{10}^{\rm SM}} \tag{71}$$

parametrizes NP effects. The relations

$$|\mathcal{C}_{10}| = \sqrt{1 + 2|\mathcal{C}_{10}^{\rm NP}| \cos\varphi_{10}^{\rm NP} + |\mathcal{C}_{10}^{\rm NP}|^2}, \tag{72}$$
$$|\mathcal{C}_{10}| \cos\varphi_{10} = 1 + |\mathcal{C}_{10}^{\rm NP}| \cos\varphi_{10}^{\rm NP},$$
$$|\mathcal{C}_{10}| \sin\varphi_{10} = |\mathcal{C}_{10}^{\rm NP}| \sin\varphi_{10}^{\rm NP}, \tag{73}$$
$$\tan\varphi_{10} = \frac{|\mathcal{C}_{10}^{\rm NP}| \sin\varphi_{10}^{\rm NP}}{1 + |\mathcal{C}_{10}^{\rm NP}| \cos\varphi_{10}^{\rm NP}} \tag{74}$$

allow us to express $\mathcal{C}_{10}$ in terms of the – in general – complex NP coefficient $\mathcal{C}_{10}^{\rm NP}$.

In order to reveal the substructure of P, information on $\mathcal{C}_{10}$ is required. In specific models, we may calculate $\mathcal{C}_{10}^{\rm NP}$ (see, for instance, Ref. [6]). Alternatively, using experimental data for $B \to K^{(*)}\ell^+\ell^-$ decays, we may determine $C_{10} - C'_{10}$ from experiment (see Ref. [28] and references therein). In practice, the corresponding NP contributions are extracted through involved global fits to sets of large numbers of observables. We use the results from Ref. [28], where different scenarios for NP in real Wilson coefficients are discussed. Considering NP in individual Wilson coefficients, the authors find that the data is best explained by a contribution to the short-distance coefficient C_9 of the four-fermion operator $O_9 = (\bar{s}\gamma_\mu P_L b)(\bar{\mu}\gamma^\mu \mu)$, which does not contribute to $B_s^0 \to \mu^+\mu^-$, yielding $\mathcal{C}_{10}^{\rm NP} = 0$ and thus $\mathcal{C}_{10} = 1$. However, a similarly good fit is obtained by assuming the relation $C_9^{\rm NP} = -C_{10}^{\rm NP}$ for real coefficients, which appears in models with new particles that couple only to left-handed leptons. In this case, we find

$$\mathcal{C}_{10}^{\rm NP} = -0.16^{+0.04}_{-0.04}, \tag{75}$$

where the minus sign follows from $C_{10}^{\rm SM}$ taking a negative value, as given in Eq. (9), resulting in

$$\mathcal{C}_{10} = 0.84^{+0.04}_{-0.04}. \tag{76}$$

In Ref. [28], CP-violating phases are neglected. However, the short-distance coefficients are in general complex, and the phases can be included in the fit. In Ref. [29], such an analysis is performed. The results are presented as 2D confidence

contours in the complex plane of the coefficients C_{10} and C'_{10}. To probe for the possible size of φ_{10} and $|\mathcal{C}_{10}|$, we assume that $C'_{10} = 0$ and convert the 1σ allowed regions for the complex Wilson coefficient C_{10} shown in Ref. [29] into $\mathcal{C}_{10}$ using Eq. (70), yielding

$$-40^\circ < \varphi_{10} < -14^\circ \quad \vee \quad 14^\circ < \varphi_{10} < 40^\circ, \tag{77}$$

$$0.79 < |\mathcal{C}_{10}| < 0.98. \tag{78}$$

Due to the structure of Eq. (74), we obtain a rather constrained range for the CP-violating phase φ_{10}. It is also interesting to note that the range for the absolute value $|\mathcal{C}_{10}|$ is consistent with the result in Eq. (76).

In the future, analyses of CP-violating effects in $B \to K^{(*)}\ell^+\ell^-$ and $B_s \to \phi\mu^+\mu^-$ observables, as introduced in Refs. [30,31], will allow us to get a much sharper picture of $|\mathcal{C}_{10}|$ and a possible complex phase φ_{10}. It would be very useful to add the complex coefficient $\mathcal{C}_{10}$ as a default output to the corresponding sophisticated fits to the semileptonic rare $B_{(s)}$ decay data.

For the numerical illustrations below, we will either use the range in Eq. (76) for real Wilson coefficients C_{10} and C'_{10}, or we will consider the case $|\mathcal{C}_{10}| = 1, \varphi_{10} = 0^\circ$, where NP effects would enter exclusively through (pseudo)-scalar contributions.

An interesting situation arises if we consider a scenario where NP effects enter only through $\mathcal{C}_{10}$, with vanishing coefficients C_P, C'_P and C_S, C'_S, yielding $P = \mathcal{C}_{10}$ and $S = 0$. Specific examples are given by models with extra Z' bosons (see, for instance, Ref. [6]) and scenarios with modified Z couplings (such as in models with vector-like quarks [32]). We would then have the simple expressions

$$\mathcal{A}^{\mu\mu}_{\Delta\Gamma_s} = \cos\left(2\varphi_{10} - \phi_s^{\rm NP}\right), \quad \mathcal{S}_{\mu\mu} = \sin\left(2\varphi_{10} - \phi_s^{\rm NP}\right) \tag{79}$$

with $\mathcal{C}_{\mu\mu} = 0$. Consequently, the observables would lie on a circle with radius one in the $\mathcal{A}^{\mu\mu}_{\Delta\Gamma_s}$–$\mathcal{S}_{\mu\mu}$ plane.

4.3 Extraction of $|x|$ and Δ

Applying the method presented in Sect. 3.1, we may determine $|S|$, $|P|$ and φ_P from the $B_s^0 \to \mu^+\mu^-$ observables as functions φ_S. Using Eq. (66), we may convert these parameters into the ratio x of the – in general – complex scalar short-distance coefficients:

$$|x|e^{i\Delta} = \frac{w(P - \mathcal{C}_{10}) + S}{w(P - \mathcal{C}_{10}) - S}, \tag{80}$$

with

$$|x| = \sqrt{\frac{w^2\,|P - \mathcal{C}_{10}|^2 + |S|^2 + 2\,w\,\Re\left[(P^* - \mathcal{C}_{10}^*)S\right]}{w^2\,|P - \mathcal{C}_{10}|^2 + |S|^2 - 2\,w\,\Re\left[(P^* - \mathcal{C}_{10}^*)S\right]}} \tag{81}$$

and

$$\cos\Delta \propto w^2|P - \mathcal{C}_{10}|^2 - |S|^2,$$
$$\sin\Delta \propto 2\,w\,\Im\left[(P^* - \mathcal{C}_{10}^*)S\right], \tag{82}$$

yielding

$$\tan\Delta = \frac{2\,w\,\Im\left[(P^* - \mathcal{C}_{10}^*)S\right]}{w^2|P - \mathcal{C}_{10}|^2 - |S|^2}. \tag{83}$$

The quantities entering these expression can be expressed in terms of the absolute values and phases of the relevant complex coefficients as

$$|P - \mathcal{C}_{10}| = \sqrt{|P|^2 - 2|P||\mathcal{C}_{10}|\cos(\varphi_{10} - \varphi_P) + |\mathcal{C}_{10}|^2} \tag{84}$$

and

$$\Im\left[(P^* - \mathcal{C}_{10}^*)S\right] = |S|\Big[|P|\sin(\varphi_S - \varphi_P) - |\mathcal{C}_{10}|\sin(\varphi_S - \varphi_{10})\Big] \tag{85}$$

$$\Re\left[(P^* - \mathcal{C}_{10}^*)S\right] = |S|\Big[|P|\cos(\varphi_S - \varphi_P) - |\mathcal{C}_{10}|\cos(\varphi_S - \varphi_{10})\Big]. \tag{86}$$

It is instructive to consider the example in Sect. 3.2.2, where $|S| = 0.30$ and $\varphi_S = 20^\circ$. Using the expressions given above, we can convert the corresponding values of $|P| = 0.89$ and $\varphi_P = 30^\circ$ into

$$|x| = 0.89, \quad \Delta = -62^\circ, \tag{87}$$

where we have assumed no NP in $\mathcal{C}_{10}$, so $|\mathcal{C}_{10}| = 1$ and $\varphi_{10} = 0^\circ$. In Fig. 5, we give a flowchart for this strategy, and show in Fig. 6 the situation corresponding to Eq. (87). Using information on the sign of $\mathcal{C}_{\mu\mu}$, we would only be left with the red contours. We observe that $|x|e^{i\Delta}$ could be constrained in a very non-trivial way. The resulting contours depend strongly on the associated $B_s^0 \to \mu^+\mu^-$ decay observables.

In order to constrain the parameters more stringently, it is useful to make assumptions about scenarios, as we will illustrate in the next section. Following these lines, we may rule out a given scenario or confirm it, allowing us then to extract the corresponding parameters. By the time we may have measurements of CP violation in $B_s^0 \to \mu^+\mu^-$ available, we should have a much better picture of the physics beyond the SM, thanks to the interplay between model building and data coming both from the high-energy and the high-precision frontiers. In particular, we should then also have

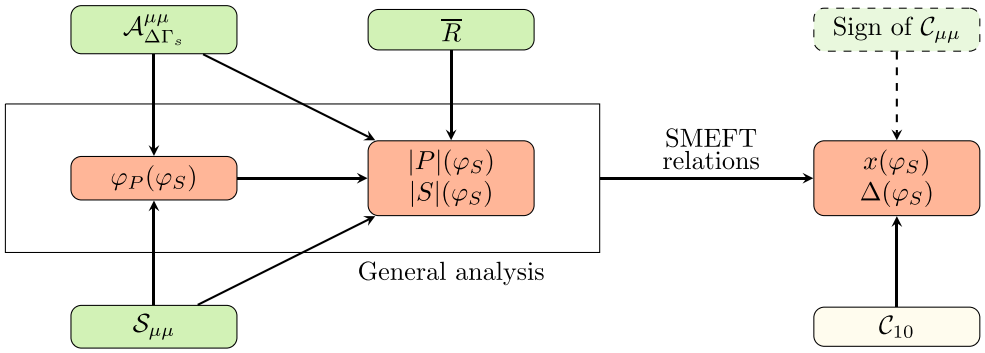

Fig. 5 Flowchart to illustrate the use of the SMEFT relations in Sect. 4.1 for the analysis of the $B_s^0 \to \mu^+\mu^-$ observables as described in the text

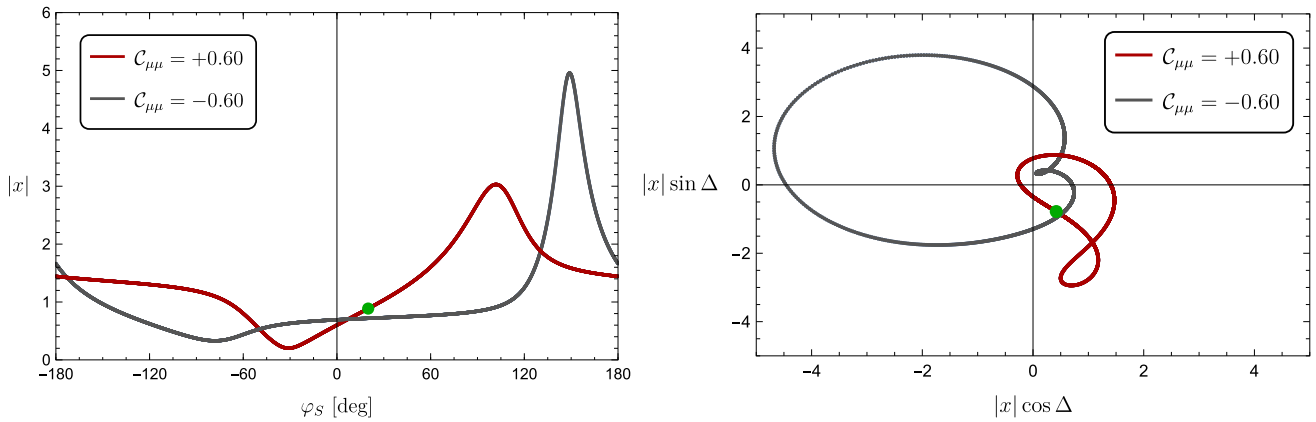

Fig. 6 Implementation of Fig. 5 for the example in Sect. 3.2.2, corresponding to Eq. (87), which is illustrated by the green dots. In the left panel, we give the resulting dependence of $|x|$ on φ_S, while in the right panel, we show $|x|e^{i\Delta}$ in the complex plane. The grey contours could be excluded through sign information for the observable $\mathcal{C}_{\mu\mu}$

some preferred scenarios, including specific patterns for the CP-violating phases, which could be confronted with experimental data and the new strategies presented in this paper.

4.4 Illustration

As experimental data have already constrained the NP contribution $\phi_s^{\rm NP}$ to the B_s^0–$\bar{B}_s^0$ mixing phase to be tiny, as given in Eq. (17), we may simplify the discussion by neglecting this quantity. Moreover, for the decay $B_s^0 \to \mu^+\mu^-$, we have with excellent precision $w = 1$. Let us now illustrate the formalism and strategy discussed above through various examples. Here we shall choose values for the input parameters to calculate the decay observables. Assuming then that these quantities have been measured at the future LHC upgrade(s), we discuss the pictures emerging from the strategy discussed above. For simplicity, we do not consider experimental aspects in this section but will illustrate scenarios assuming uncertainties of future measurements in Sect. 5.

4.4.1 $x = 0$ *and* $|x| \to \infty$

The case $x = 0$, which corresponds to $C_S' = C_P' = 0$, is frequently considered in the literature for vanishing CP-violating phases (see, for instance, Ref. [7]). It is interesting to note that the relation in Eq. (69) gives

$$w\,P + S = w\,\mathcal{C}_{10}, \tag{88}$$

which reduces to $P + S = 1$ for $w = 1$ and $\mathcal{C}_{10} = 1$. Allowing for possible CP violation, using the expressions in the Appendix we obtain

$$r|_{x=0} = |\mathcal{C}_{10}|^2 - 2\cos(\varphi_{10} - \varphi_S)|\mathcal{C}_{10}||S| + 2|S|^2 \tag{89}$$

as well as

$$\mathcal{A}^{\mu\mu}_{\Delta\Gamma_s}|_{x=0} = \frac{|\mathcal{C}_{10}|^2\cos 2\varphi_{10} - 2\cos(\varphi_{10} + \varphi_S)|\mathcal{C}_{10}||S|}{|\mathcal{C}_{10}|^2 - 2\cos(\varphi_{10} - \varphi_S)|\mathcal{C}_{10}||S| + 2|S|^2} \tag{90}$$

$$\mathcal{S}_{\mu\mu}|_{x=0} = \frac{|\mathcal{C}_{10}|^2\sin 2\varphi_{10} - 2\sin(\varphi_{10} + \varphi_S)|\mathcal{C}_{10}||S|}{|\mathcal{C}_{10}|^2 - 2\cos(\varphi_{10} - \varphi_S)|\mathcal{C}_{10}||S| + 2|S|^2} \tag{91}$$

$$\mathcal{C}_{\mu\mu}|_{x=0} = \frac{2|S|\,[|\mathcal{C}_{10}|\cos(\varphi_{10}-\varphi_S)-|S|]}{|\mathcal{C}_{10}|^2-2\cos(\varphi_{10}-\varphi_S)|\mathcal{C}_{10}||S|+2|S|^2}. \quad (92)$$

Using Eq. (38), and substituting r and $\mathcal{A}^{\mu\mu}_{\Delta\Gamma_s}$ according to Eqs. (89) and (90), we may determine $|S|$ as a function of $\varphi_{10}-\varphi_S$ from the measured value of $\overline{R}$:

$$|S| = \frac{|\mathcal{C}_{10}|}{2}\left\{[\cos(\varphi_{10}-\varphi_S)+y_s\cos(\varphi_{10}+\varphi_S)] \pm \sqrt{[\cos(\varphi_{10}-\varphi_S)+y_s\cos(\varphi_{10}+\varphi_S)]^2-2\left[1+y_s\cos 2\varphi_{10}-\frac{\overline{R}}{|\mathcal{C}_{10}|^2}(1+y_s)\right]}\right\}. \quad (93)$$

Note that the discriminant must have a value greater than or equal to zero, which implies the following upper bound:

$$|\mathcal{C}_{10}| \le \sqrt{\left(\frac{2}{1-y_s}\right)\overline{R}}. \quad (94)$$

The current experimental value of $\overline{R}$ in Eq. (28) yields

$$|\mathcal{C}_{10}| \le 1.3 \pm 0.1, \quad (95)$$

which is obviously consistent with $\mathcal{C}_{10}=1$.

The number of allowed solutions for a given angle φ_S depends on the value of the Wilson coefficient $\mathcal{C}_{10}$. In order to illustrate this feature, we consider two scenarios for $\mathcal{C}_{10}$. Let us first assume that there is a vanishing NP contribution $\mathcal{C}_{10}^{\rm NP}=0$, which yields $|\mathcal{C}_{10}|=1,\ \varphi_{10}=0°$. In this case, Eq. (93) results in two solutions for $|S|$ as a function of φ_S, as can be seen in the top-left plot in Fig. 7. Using Eqs. (90), (91) and (92), we can determine the observables $\mathcal{A}^{\mu\mu}_{\Delta\Gamma_s}$, $\mathcal{S}^{\mu\mu}$ and $\mathcal{C}_{\mu\mu}$ as functions of φ_S, respectively, as shown in Fig. 7. In

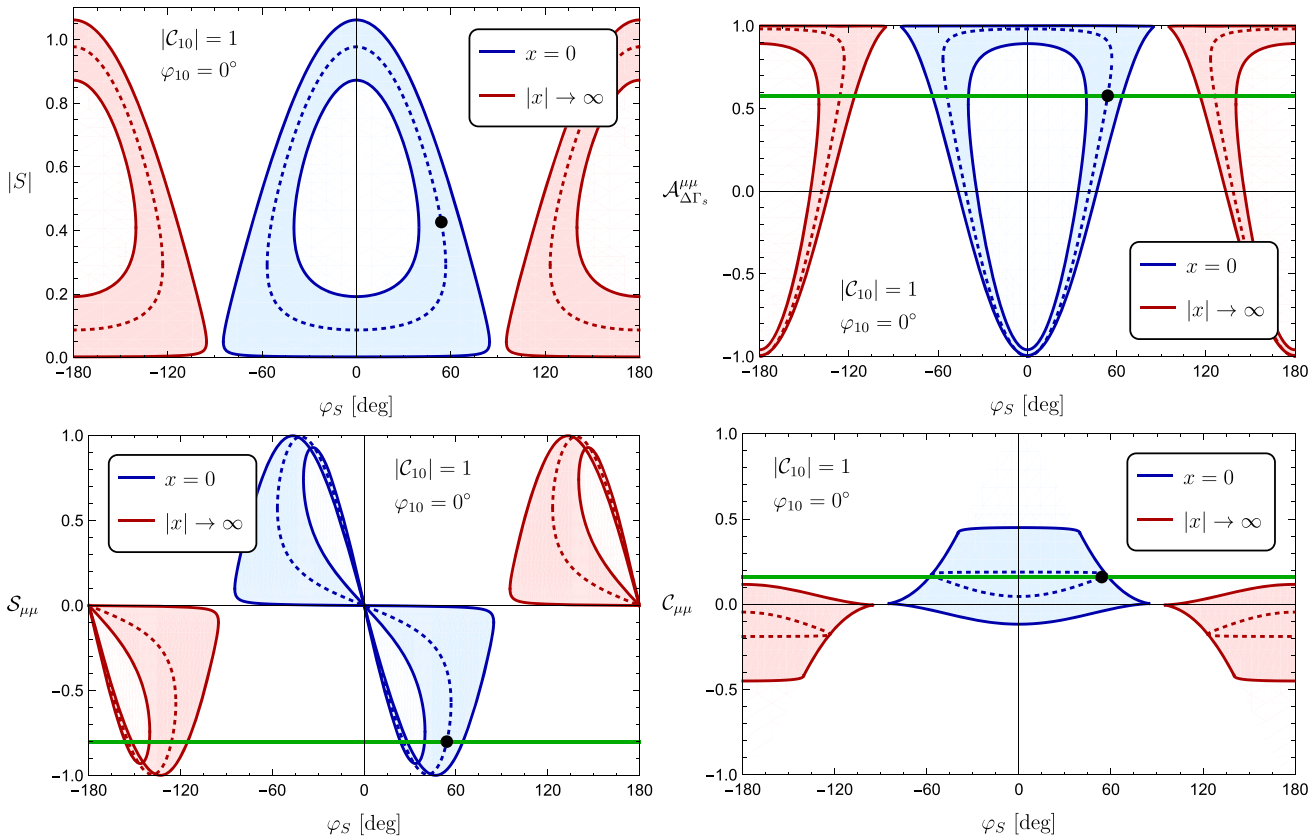

Fig. 7 Functional dependences between $|S|$, $\mathcal{A}^{\mu\mu}_{\Delta\Gamma_s}$, $\mathcal{S}_{\mu\mu}$, $\mathcal{C}_{\mu\mu}$ and the CP-violating phase φ_S for $|\mathcal{C}_{10}|=1,\ \varphi_{10}=0°$. The blue and red contours correspond to the scenarios $x=0$ and $|x|\to\infty$, respectively. The allowed regions are determined within the $1\,\sigma$ range for $\overline{R}$ given in Eq. (28), where the dashed curve is associated with the central value for this observable. Notice that for each value of φ_S, we have in general two possible solutions for the observables, leading to closed loops in the parameter space. The black dot refers to the input parameters of the scenario in Eq. (104), whereas the green line shows the value of the observables in Eq. (107)

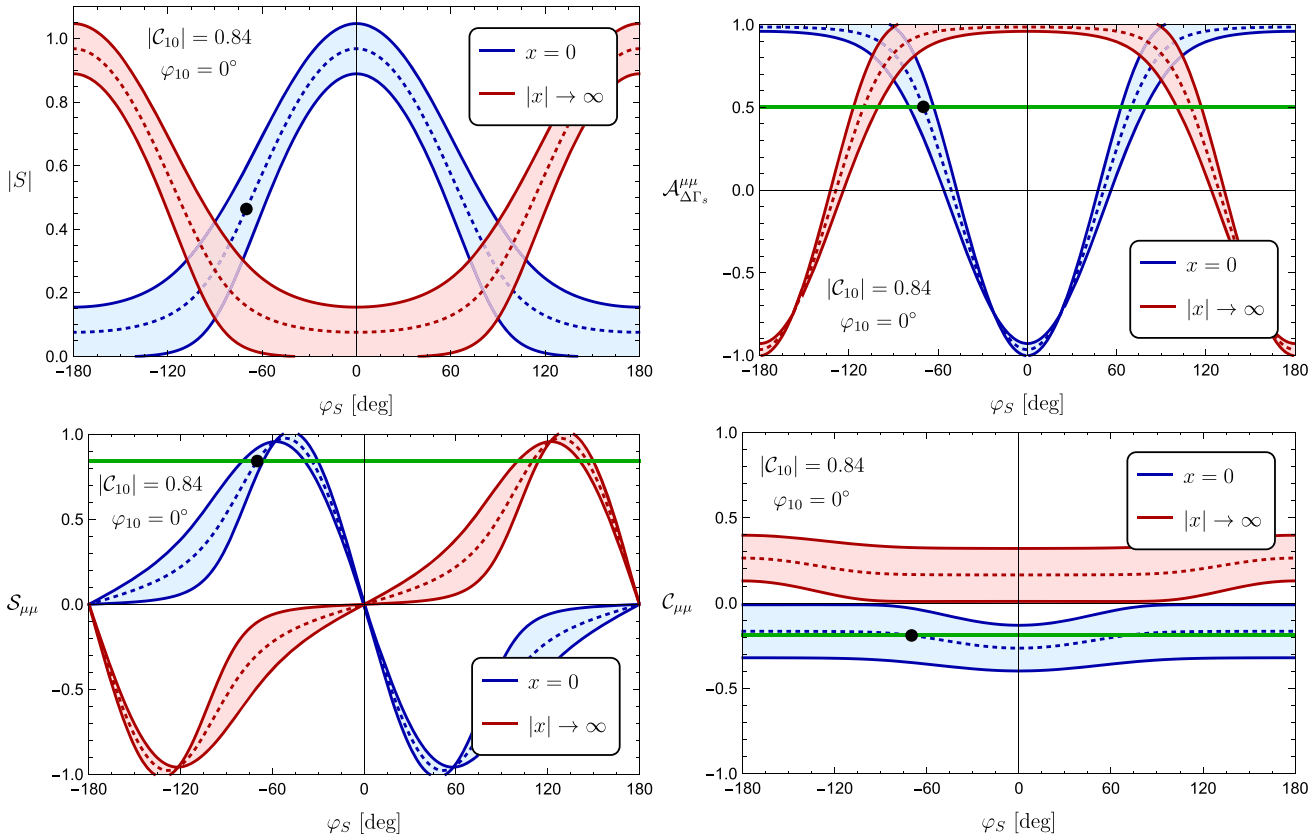

Fig. 8 Functional dependences between $|S|$, $\mathcal{A}^{\mu\mu}_{\Delta\Gamma_s}$, $\mathcal{S}_{\mu\mu}$, $\mathcal{C}_{\mu\mu}$ and the CP-violating phase φ_S for $|\mathcal{C}_{10}| = 0.84$ and $\varphi_{10} = 0°$. The blue and red contours correspond to the scenarios $x = 0$ and $|x| \to \infty$, respectively. The allowed regions are determined within the $1\,\sigma$ range for $\overline{R}$ given in Eq. (28), where the dashed curve is associated with the central value for this observable. The black dot refers to the input parameters of the scenario in Eq. (108), whereas the green line shows the value of the observables in Eq. (111)

particular, once $\mathcal{A}^{\mu\mu}_{\Delta\Gamma_s}$ has been measured, the value of $\mathcal{S}_{\mu\mu}$ can be predicted. Should this CP asymmetry be measured correspondingly, this scenario would be confirmed, allowing us to determine the corresponding NP parameters. On the other hand, should the measurement of $\mathcal{S}_{\mu\mu}$ be in conflict with the prediction, the NP scenario would be ruled out by experimental data.

Let us now consider a scenario with NP contributions to $\mathcal{C}_{10}$. If we follow the analysis of Ref. [28] and use the central value of $\mathcal{C}_{10}$ in Eq. (76), we obtain the functional dependence of $|S|$ and the corresponding observables on φ_S shown Fig. 8. Interestingly, for a given value of φ_S, Eq. (93) gives now a single solution for $|S|$. Consequently, unlike their counterparts in Fig. 7, the contours no longer form closed loops, thereby indicating that the degeneracy with respect to φ_S has disappeared. In Fig. 9, we illustrate this strategy, which is actually more general, i.e. does not only apply to the case of $x = 0$.

A closer look at the expressions in the Appendix shows that the case of $x = 0$ is connected with $|x| \to \infty$, where the scalar and pseudo-scalar coefficients C_S and C_P vanish while $C'_P = C'_S$ takes a non-vanishing value. The expression in Eq. (69) takes then the form

$$w\,P - S = w\,\mathcal{C}_{10}, \tag{96}$$

which reduces to $P - S = 1$ for $w = 1$ and $\mathcal{C}_{10} = 1$. For the observables r as well as $\mathcal{A}^{\mu\mu}_{\Delta\Gamma_s}$ and $\mathcal{S}_{\mu\mu}$, we have the symmetry relation

$$\varphi_S \to \pi + \varphi_S, \tag{97}$$

which is equivalent to $|S| \to -|S|$, and yields

$$r|_{|x|\to\infty} = |\mathcal{C}_{10}|^2 + 2\cos(\varphi_{10} - \varphi_S)|\mathcal{C}_{10}||S| + 2|S|^2 \tag{98}$$

$$\mathcal{A}^{\mu\mu}_{\Delta\Gamma_s}|_{|x|\to\infty} = \frac{|\mathcal{C}_{10}|^2\cos 2\varphi_{10} + 2\cos(\varphi_{10} + \varphi_S)|\mathcal{C}_{10}||S|}{|\mathcal{C}_{10}|^2 + 2\cos(\varphi_{10} - \varphi_S)|\mathcal{C}_{10}||S| + 2|S|^2} \tag{99}$$

$$\mathcal{S}_{\mu\mu}|_{|x|\to\infty} = \frac{|\mathcal{C}_{10}|^2\sin 2\varphi_{10} + 2\sin(\varphi_{10} + \varphi_S)|\mathcal{C}_{10}||S|}{|\mathcal{C}_{10}|^2 + 2\cos(\varphi_{10} - \varphi_S)|\mathcal{C}_{10}||S| + 2|S|^2}. \tag{100}$$

In the case of $\mathcal{C}_{\mu\mu}$, the symmetry is broken by an overall minus sign:

$$\mathcal{C}_{\mu\mu}|_{|x|\to\infty} = \frac{2|S|\,[|\mathcal{C}_{10}|\cos(\varphi_{10} - \varphi_S) + |S|]}{|\mathcal{C}_{10}|^2 + 2\cos(\varphi_{10} - \varphi_S)|\mathcal{C}_{10}||S| + 2|S|^2}. \tag{101}$$

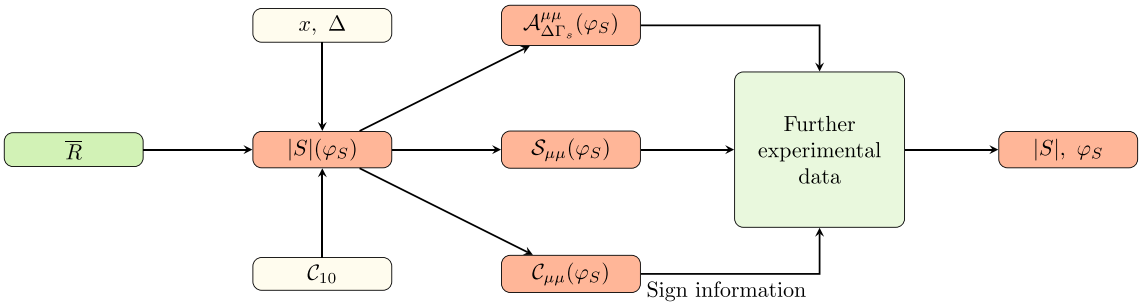

Fig. 9 Flowchart to illustrate the use of the relations in Sect. 4.1 with information on $\mathcal{C}_{10}$ to convert the measured value of $\overline{R}$ into predictions of the $B_s^0 \to \mu^+\mu^-$ observables. Once these are measured in accordance with the pattern characterizing the NP scenario, $|S|$ and φ_S can be extracted from the data

More explicitly, we have

$$\begin{aligned} r|_{x=0}(\varphi_S+\pi) &= r|_{|x|\to\infty}(\varphi_S) \\ \mathcal{A}^{\mu\mu}_{\Delta\Gamma_s}|_{x=0}(\varphi_S+\pi) &= \mathcal{A}^{\mu\mu}_{\Delta\Gamma_s}|_{|x|\to\infty}(\varphi_S) \\ \mathcal{S}_{\mu\mu}|_{x=0}(\varphi_S+\pi) &= \mathcal{S}_{\mu\mu}|_{|x|\to\infty}(\varphi_S), \end{aligned} \tag{102}$$

while

$$\mathcal{C}_{\mu\mu}|_{x=0}(\varphi_S+\pi) = -\mathcal{C}_{\mu\mu}|_{|x|\to\infty}(\varphi_S). \tag{103}$$

As we will see below, this feature has interesting phenomenological implications.

In order to illustrate the expressions given above, we consider two examples with different values of the coefficient $\mathcal{C}_{10}$:

Example (a)

We first assume a situation with vanishing NP contributions $\mathcal{C}_{10}^{\rm NP} = 0$, and employ the following setup:

$$\begin{aligned} &\overline{R} = 0.84 \pm 0.16, \quad x = 0, \quad \varphi_S = 54^\circ, \\ &|\mathcal{C}_{10}| = 1, \quad \varphi_{10} = 0^\circ. \end{aligned} \tag{104}$$

Using Eq. (93), we determine $|S|$ as a function of φ_S. As discussed above, for $|\mathcal{C}_{10}| = 1$, $\varphi_{10} = 0^\circ$ and the central value of $\overline{R}$ in Eq. (104), we obtain a twofold solution. For the sake of illustration, we consider only the solution with the plus sign in front of the square root, yielding

$$|S| = 0.43. \tag{105}$$

With the help of Eq. (66), we may now calculate

$$|P| = 0.82, \quad \varphi_P = -25^\circ. \tag{106}$$

The corresponding values for the observables read as follows:

$$\mathcal{A}^{\mu\mu}_{\Delta\Gamma_s} = 0.58, \quad \mathcal{S}_{\mu\mu} = -0.80, \quad \mathcal{C}_{\mu\mu} = 0.16. \tag{107}$$

Let us now assume that these observables have been measured, and discuss how we may then – with the help of the strategy discussed above – reveal the dynamics of the $B_s^0 \to \mu^+\mu^-$ decay and distinguish between the $x = 0$ and $|x| \to \infty$ cases:

- It is plausible to expect that $\mathcal{A}^{\mu\mu}_{\Delta\Gamma_s}$ is the next observable to be measured. With the help of the top-right plot in Fig. 7, we identify four possible values for φ_S which are compatible with the "experimental" result of $\mathcal{A}^{\mu\mu}_{\Delta\Gamma_s} = 0.58$ in Eq. (107): $\varphi_S^{(1)} = -126^\circ$, $\varphi_S^{(2)} = -54^\circ$, $\varphi_S^{(3)} = 54^\circ$ and $\varphi_S^{(4)} = 126^\circ$.
- We may now predict the observable $\mathcal{S}_{\mu\mu}$. Using the bottom-left plot in Fig. 7 or the expressions in Eqs. (91) and (100), we obtain $\mathcal{S}_{\mu\mu} = -0.80$ for $\varphi_S^{(1)} = -126^\circ$ (branch $|x| \to \infty$) and $\varphi_S^{(3)} = 54^\circ$ (branch $x = 0$). Moreover, we find $\mathcal{S}_{\mu\mu} = 0.80$ for $\varphi_S^{(2)} = -54^\circ$ (branch $x = 0$) and $\varphi_S^{(4)} = 126^\circ$ (branch $|x| \to \infty$).
- The measurement $\mathcal{S}_{\mu\mu} = -0.80$ would then allow us to narrow down the four solutions for φ_S to only two at $\varphi_S^{(1)} = -126^\circ$ and $\varphi_S^{(3)} = 54^\circ$, corresponding to $|x| \to \infty$ and $x = 0$, respectively. It should be emphasized that both solutions would be valid at this stage of the analysis, i.e. we would have confirmed a CP-violating NP scenario with either $|x| \to \infty$ or $x = 0$.
- This ambiguity can be resolved through information on the sign of $\mathcal{C}_{\mu\mu}$, which is given by $\mathcal{C}_{\mu\mu} = -0.16$ and $\mathcal{C}_{\mu\mu} = +0.16$ for $|x| \to \infty$ and $x = 0$, respectively, as can be seen in Fig. 7. Consequently, the fact that $\mathcal{C}_{\mu\mu}$ breaks the symmetry in Eq. (97) gives us a powerful tool to distinguish between $x = 0$ and $|x| \to \infty$.

Example (b)

Now we have a look at a scenario with NP contributions to $\mathcal{C}_{10}$, which is characterized as follows:

$$\begin{aligned} &\overline{R} = 0.84 \pm 0.16, \quad x = 0, \quad \varphi_S = -70^\circ, \\ &|\mathcal{C}_{10}| = 0.84, \quad \varphi_{10} = 0^\circ. \end{aligned} \tag{108}$$

Here the value of $\mathcal{C}_{10}$ follows from Eq. (76), and is discussed in more detail in Sect. 4.2. In contrast to Example (a), we obtain now a single solution for $|S|$ from Eq. (93), which is

given by

$$|S| = 0.46. \tag{109}$$

Using Eq. (66), we find

$$|P| = 0.81, \quad \varphi_P = 33^\circ, \tag{110}$$

resulting in the following values of the observables:

$$\mathcal{A}^{\mu\mu}_{\Delta\Gamma_s} = 0.50, \quad \mathcal{S}_{\mu\mu} = 0.84, \quad \mathcal{C}_{\mu\mu} = -0.19. \tag{111}$$

In analogy to Example (a), using the plots in Fig. 8, we may again show the compatibility of the "measured" observables with the scenario $x = 0$, and rule out the case of $|x| \to \infty$ through the sign of the $\mathcal{C}_{\mu\mu}$ asymmetry. For the convenience of the reader, we summarize the main features of these examples in Table 1.

In Fig. 10, we show the correlation between $\mathcal{A}^{\mu\mu}_{\Delta\Gamma_s}$ and $\mathcal{S}_{\mu\mu}$ through the CP-violating phase φ_S. It should be noted that the corresponding regions for $|\mathcal{C}_{10}| = 0.84$, $\varphi_{10} = 0^\circ$ and $|\mathcal{C}_{10}| = 1$, $\varphi_{10} = 0^\circ$ do not differ substantially and are included in a single plot. Due to the symmetry transformation in Eq. (97), the scenarios $x = 0$ and $|x| \to \infty$ cover the same region once we make a scan over the full range of φ_S. The allowed region in Fig. 10 exhibits the following interesting features:

1. The currently available measurement of $\overline{R}$ implies a remarkably constrained circular region in the $\mathcal{A}^{\mu\mu}_{\Delta\Gamma_s}$–$\mathcal{S}_{\mu\mu}$ plane for CP-violating NP scenarios characterized by $x = 0$ and $|x| \to \infty$.
2. A future measurement of the observable combination $\mathcal{A}^{\mu\mu}_{\Delta\Gamma_s}$ and $\mathcal{S}_{\mu\mu}$ lying outside the allowed region would rule out the $x = 0$ and $|x| \to \infty$ scenarios.
3. The allowed region in the $\mathcal{A}^{\mu\mu}_{\Delta\Gamma_s}$–$\mathcal{S}_{\mu\mu}$ plane is close to the unit circle. Consequently, due to Eq. (1), the observable $\mathcal{C}_{\mu\mu}$ is constrained to take a smallish value.
4. The allowed region is similar to the one arising for the scenario described in Sect. 4.2. While here $\varphi_{10} = 0^\circ$ would imply the SM results $\mathcal{A}^{\mu\mu}_{\Delta\Gamma_s} = 1$ and $\mathcal{S}_{\mu\mu} = 0$, in the case of $x = 0$ or $|x| \to \infty$ we may still deviate substantially from the SM even in spite of having a vanishing phase φ_{10}.

In a complementary way, if we can obtain the value of the phase φ_S from external information or theoretical considerations, we will be able to predict the observables $\mathcal{A}^{\mu\mu}_{\Delta\Gamma_s}$ and $\mathcal{S}_{\mu\mu}$ compatible with vanishing short distance contributions $C_{P,S}$ or $C'_{P,S}$. Strong deviations from these determinations will indicate that the corresponding scenarios are not realized in Nature. A discussion of NP scenarios characterized by the relations $P \pm S = 1$ (see Eqs. (88) and (96)) can be found in Ref. [6].

4.4.2 $\Delta = 0^\circ$

Another interesting case arises if C'_S and C_S have the same CP-violating phases, i.e. $\Delta = 0^\circ$, which yields

$$r|_{\Delta=0^\circ} = |\mathcal{C}_{10}|^2 - 2\left(\frac{1+|x|}{1-|x|}\right)\cos(\varphi_{10}-\varphi_S)|\mathcal{C}_{10}||S| + 2\left[\frac{1+|x|^2}{(1-|x|)^2}\right]|S|^2 \tag{112}$$

$$\mathcal{A}^{\mu\mu}_{\Delta\Gamma_s}|_{\Delta=0^\circ} = \frac{(1-|x|)^2|\mathcal{C}_{10}|^2\cos 2\varphi_{10} - 2\left(1-|x|^2\right)\cos(\varphi_{10}+\varphi_S)|\mathcal{C}_{10}||S| + 4|x||S|^2\cos 2\varphi_S}{(1-|x|)^2|\mathcal{C}_{10}|^2 - 2\left(1-|x|^2\right)\cos(\varphi_{10}-\varphi_S)|\mathcal{C}_{10}||S| + 2(1+|x|^2)|S|^2} \tag{113}$$

$$\mathcal{S}_{\mu\mu}|_{\Delta=0^\circ} = \frac{(1-|x|)^2|\mathcal{C}_{10}|^2\sin 2\varphi_{10} - 2\left(1-|x|^2\right)\sin(\varphi_{10}+\varphi_S)|\mathcal{C}_{10}||S| + 4|x||S|^2\sin 2\varphi_S}{(1-|x|)^2|\mathcal{C}_{10}|^2 - 2\left(1-|x|^2\right)\cos(\varphi_{10}-\varphi_S)|\mathcal{C}_{10}||S| + 2(1+|x|^2)|S|^2} \tag{114}$$

$$\mathcal{C}_{\mu\mu}|_{\Delta=0^\circ} = \frac{2|S|\left[(1-|x|)^2|\mathcal{C}_{10}|\cos(\varphi_{10}-\varphi_S) - (1-|x|^2)|S|\right]}{(1-|x|)^2|\mathcal{C}_{10}|^2 - 2\left(1-|x|^2\right)\cos(\varphi_{10}-\varphi_S)|\mathcal{C}_{10}||S| + 2(1+|x|^2)|S|^2}. \tag{115}$$

In analogy to the scenarios $x = 0$ and $|x| \to \infty$ discussed in Sect. 4.4.1, the expressions in Eqs. (112)–(114) are invariant under the symmetry transformation

$$|x| \to 1/|x|, \quad \varphi_S \to \varphi_S + \pi, \tag{116}$$

leading to

$$\begin{aligned} r|_{\Delta=0^\circ}(|x|,\varphi_S) &= r|_{\Delta=0^\circ}(1/|x|,\varphi_S+\pi) \\ \mathcal{A}^{\mu\mu}_{\Delta\Gamma_s}|_{\Delta=0^\circ}(|x|,\varphi_S) &= \mathcal{A}^{\mu\mu}_{\Delta\Gamma_s}|_{\Delta=0^\circ}(1/|x|,\varphi_S+\pi) \\ \mathcal{S}_{\mu\mu}|_{\Delta=0^\circ}(|x|,\varphi_S) &= \mathcal{S}_{\mu\mu}|_{\Delta=0^\circ}(1/|x|,\varphi_S+\pi), \end{aligned} \tag{117}$$

while the symmetry is again broken by the observable $\mathcal{C}_{\mu\mu}$ through an overall sign change:

$$\mathcal{C}_{\mu\mu}|_{\Delta=0^\circ}(|x|,\varphi_S) = -\mathcal{C}_{\mu\mu}|_{\Delta=0^\circ}(1/|x|,\varphi_S+\pi). \tag{118}$$

The three observables r, $\mathcal{A}^{\mu\mu}_{\Delta\Gamma_s}$ and $\mathcal{S}_{\mu\mu}$ in Eqs. (112)–(114) depend on the three unknowns x, $|S|$ and φ_S. Consequently, if the observables are measured, we may determine

Table 1 Summary of the strategy followed in Examples (a) and (b) to disentangle the scenario $x = 0$ from $|x| \to \infty$ and determine the value of φ_S

Observables	Solutions	Scenario
Example (a)		
$\lvert\mathcal{C}_{10}\rvert = 1, \quad \varphi_{10} = 0°$		
$\overline{R} = 0.84 \pm 0.16, \quad \mathcal{A}^{\mu\mu}_{\Delta\Gamma_s} = 0.58, \quad \mathcal{S}_{\mu\mu} = -0.80, \quad \mathcal{C}_{\mu\mu} = 0.16$		
$\mathcal{A}^{\mu\mu}_{\Delta\Gamma_s}$	$\varphi_S^{(1)} = -126°, \quad \varphi_S^{(4)} = 126°$	$\lvert x\rvert \to \infty \quad (C_S = C_P = 0)$
	$\varphi_S^{(2)} = -54°, \quad \varphi_S^{(3)} = 54°$	$x = 0 \quad (C'_S = C'_P = 0)$
$\mathcal{A}^{\mu\mu}_{\Delta\Gamma_s}, \quad \mathcal{S}_{\mu\mu}$	$\varphi_S^{(1)} = -126°$	$\lvert x\rvert \to \infty \quad (C_S = C_P = 0)$
	$\varphi_S^{(3)} = 54°$	$x = 0 \quad (C'_S = C'_P = 0)$
$\mathcal{A}^{\mu\mu}_{\Delta\Gamma_s}, \quad \mathcal{S}_{\mu\mu}, \quad \mathcal{C}_{\mu\mu}$	$\varphi_S^{(3)} = 54°$	$x = 0 \quad (C'_S = C'_P = 0)$
Example (b)		
$\lvert\mathcal{C}_{10}\rvert = 0.84, \quad \varphi_{10} = 0°$		
$\overline{R} = 0.84 \pm 0.16, \quad \mathcal{A}^{\mu\mu}_{\Delta\Gamma_s} = 0.50, \quad \mathcal{S}_{\mu\mu} = 0.84, \quad \mathcal{C}_{\mu\mu} = -0.19$		
$\mathcal{A}^{\mu\mu}_{\Delta\Gamma_s}$	$\varphi_S^{(1)} = -110°, \quad \varphi_S^{(4)} = 110°$	$\lvert x\rvert \to \infty \quad (C_S = C_P = 0)$
	$\varphi_S^{(2)} = -70°, \quad \varphi_S^{(3)} = 70°$	$x = 0 \quad (C'_S = C'_P = 0)$
$\mathcal{A}^{\mu\mu}_{\Delta\Gamma_s}, \quad \mathcal{S}_{\mu\mu}$	$\varphi_S^{(4)} = 110°$	$\lvert x\rvert \to \infty \quad (C_S = C_P = 0)$
	$\varphi_S^{(2)} = -70°$	$x = 0 \quad (C'_S = C'_P = 0)$
$\mathcal{A}^{\mu\mu}_{\Delta\Gamma_s}, \quad \mathcal{S}_{\mu\mu}, \quad \mathcal{C}_{\mu\mu}$	$\varphi_S^{(2)} = -70°$	$x = 0 \quad (C'_S = C'_P = 0)$

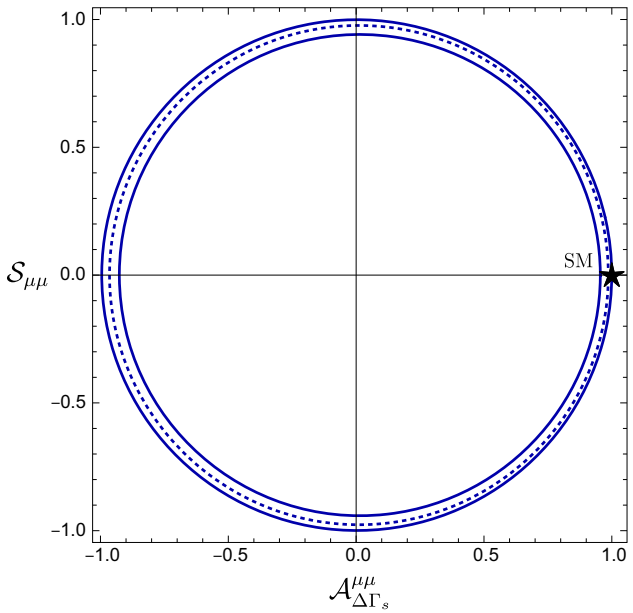

Fig. 10 Allowed region in the $\mathcal{A}^{\mu\mu}_{\Delta\Gamma_s}$–$\mathcal{S}_{\mu\mu}$ plane following from the current experimental value of $\overline{R}$ for $x = 0$; the same correlation is obtained for $|x| \to \infty$. The circular region corresponds to the 1σ uncertainty of $\overline{R}$ in Eq. (28). The black star indicates the SM point

these parameters. The twofold ambiguity following from the symmetry transformation in Eq. (116) can be resolved through the measurement of the sign of $\mathcal{C}_{\mu\mu}$. Unfortunately, in view of the highly non-linear structure of the equations, we cannot give simple analytic solutions. However, the parameters can be determined numerically. In Sect. 5, we will illustrate this determination through fits to scenarios of future measurements.

Alternatively, we can apply the strategy depicted in the flowchart in Fig. 9. We start with the experimental value of $\overline{R}$ given in Eq. (28). Furthermore, we assume that $|x| = 0.5$ and $|\mathcal{C}_{10}| = 1$, $\varphi_{10} = 0°$. This allows us to solve for $|S|$ as a function of φ_S, and to subsequently determine $\mathcal{A}^{\mu\mu}_{\Delta\Gamma_s}$, $\mathcal{S}_{\mu\mu}$ and $\mathcal{C}_{\mu\mu}$ as functions of φ_S. The results are shown as the blue contours in Fig. 11. Here, also the symmetric situation with $|x| = 2$ is shown in red, illustrating nicely how $\mathcal{C}_{\mu\mu}$ breaks the symmetry.

Finally, in Fig. 12, we show the correlation between $\mathcal{A}^{\mu\mu}_{\Delta\Gamma_s}$ and $\mathcal{S}_{\mu\mu}$ for $|x| = 0.5$ and $|x| = 3$. Contrary to the situation for $x = 0$, $|x| \to \infty$, we are not constrained to a contour close to the unit circle, but can also obtain values in the interior region. For the scenario $|x| = 3$, the relations $|S|$, $\mathcal{A}^{\mu\mu}_{\Delta\Gamma_s}$, $\mathcal{S}_{\mu\mu}$ and $\mathcal{C}_{\mu\mu}$ as functions of φ_S are similar to the ones shown in Fig. 11.

In the expression for r given in Eq. (112), a pole seems to arise for $|x| = 1$, which corresponds to

$$C_S = C'_S. \tag{119}$$

However, this is a spurious divergence, which is cancelled by the $C_S - C'_S$ term in the expression for S in Eq. (6), implying

$$S|_{|x|=1,\ \Delta=0°} = 0. \tag{120}$$

Using the relations in Eqs. (63) and (64), we obtain

$$C'_P = C'_S = C_S = -C_P. \tag{121}$$

Consequently, Eq. (5) yields

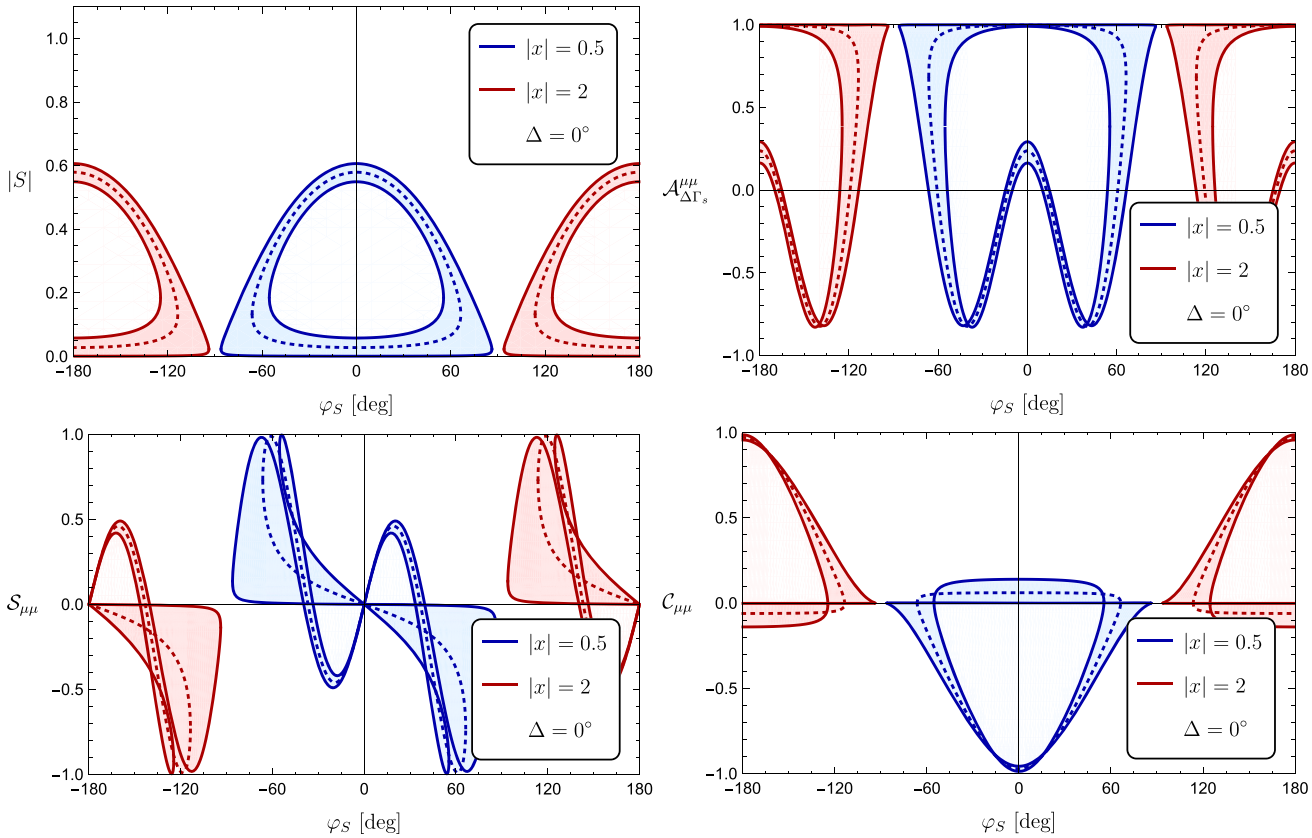

Fig. 11 Functional dependences between $|S|$, $\mathcal{A}^{\mu\mu}_{\Delta\Gamma_s}$, $\mathcal{S}_{\mu\mu}$, $\mathcal{C}_{\mu\mu}$ and the CP-violating phase φ_S for $|\mathcal{C}_{10}| = 1$, $\varphi_{10} = 0°$ and $\Delta = 0°$. The blue and red contours correspond to the scenarios $|x| = 0.5$ and the associated value $|x| = 2$, respectively. The allowed regions are determined within the $1\,\sigma$ range for $\overline{R}$ given in Eq. (28), where the dashed curve corresponds to the central value for this observable. Notice that for each value of φ_S we have in general two possible solutions for the observables, leading to closed loops in the parameter space

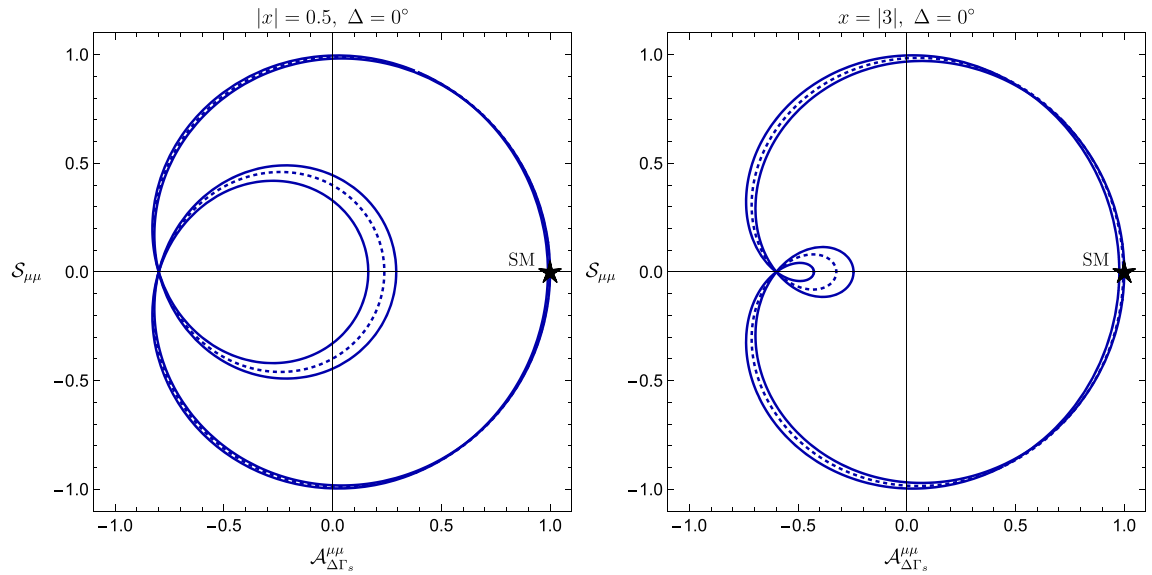

Fig. 12 Correlations between $\mathcal{A}^{\mu\mu}_{\Delta\Gamma_s}$ and $\mathcal{S}_{\mu\mu}$ in the case of $\Delta = 0°$ for $|x| = 0.5$ and $|x| = 3$ in the left and right panels, respectively. The region corresponds to the 1σ uncertainty of $\overline{R}$ in Eq. (28). The black star indicates the SM point

$$|P|e^{i\varphi_P}|_{|x|=1,\ \Delta=0^\circ} = \mathcal{C}_{10} - \frac{M_{B_s}^2}{m_\mu}\left(\frac{m_b}{m_b+m_s}\right)\frac{C_S}{C_{10}^{\rm SM}} = |\mathcal{C}_{10}|e^{i\varphi_{10}} - \frac{M_{B_s}^2}{m_\mu}\left(\frac{m_b}{m_b+m_s}\right)\frac{|C_S|}{C_{10}^{\rm SM}}e^{i\tilde{\varphi}_S} \tag{122}$$

and shows that also the divergence in Eq. (66) for $|x| = 1,\ \Delta = 0^\circ$ is spurious. If we neglect, for simplicity, again the tiny NP contribution $\phi_s^{\rm NP}$ to the B_s^0–$\bar{B}_s^0$ mixing phase, we obtain

$$r|_{|x|=1,\ \Delta=0^\circ} = |P|^2 \tag{123}$$
$$\mathcal{A}_{\Delta\Gamma_s}^{\mu\mu}|_{|x|=1,\ \Delta=0^\circ} = \cos(2\varphi_P) \tag{124}$$
$$\mathcal{S}_{\mu\mu}|_{|x|=1,\ \Delta=0^\circ} = \sin(2\varphi_P) \tag{125}$$
$$\mathcal{C}_{\mu\mu}|_{|x|=1,\ \Delta=0^\circ} = 0. \tag{126}$$

For a discussion of NP models describing this situation, see Ref. [6]. Obviously, also extensions of the SM with scalars, which couple in a left-right-symmetric way to quarks (see the operators in Eq. (3) and the relations in Eq. (119)), fall into this category.

As in the case given by Eq. (79), the correlation between the observables $\mathcal{A}_{\Delta\Gamma_s}^{\mu\mu}$ and $\mathcal{S}_{\mu\mu}$ describes a circle with radius one. The overall phase φ_P includes effects from the, in general, complex quantities $\mathcal{C}_{10}$ and C_S. This is particularly interesting if future measurements reveal $(\mathcal{A}_{\Delta\Gamma_s}^{\mu\mu})^2+(\mathcal{S}_{\mu\mu})^2$ compatible with the unit circle and if we have bounds available on the phase φ_{10} from other processes. Then, results incompatible with Eq. (79) will indicate the potential presence of a scalar or pseudo-scalar contribution.

4.4.3 $\Delta = 180^\circ$

In the case of $\Delta = 180^\circ$, we obtain the following expressions for the $B_s^0 \to \mu^+\mu^-$ observables:

$$r|_{\Delta=180^\circ} = |\mathcal{C}_{10}|^2 - 2\left(\frac{1-|x|}{1+|x|}\right)\cos(\varphi_{10}-\varphi_S)|\mathcal{C}_{10}||S| + 2\left[\frac{1+|x|^2}{(1+|x|)^2}\right]|S|^2 \tag{127}$$

$$\mathcal{A}_{\Delta\Gamma_s}^{\mu\mu}|_{\Delta=180^\circ} = \frac{(1+|x|)^2|\mathcal{C}_{10}|^2\cos 2\varphi_{10} - 2\left(1-|x|^2\right)\cos(\varphi_{10}+\varphi_S)|\mathcal{C}_{10}||S| - 4|x||S|^2\cos 2\varphi_S}{(1+|x|)^2|\mathcal{C}_{10}|^2 - 2\left(1-|x|^2\right)\cos(\varphi_{10}-\varphi_S)|\mathcal{C}_{10}||S| + 2(1+|x|^2)|S|^2} \tag{128}$$

$$\mathcal{S}_{\mu\mu}|_{\Delta=180^\circ} = \frac{(1+|x|)^2|\mathcal{C}_{10}|^2\sin 2\varphi_{10} - 2\left(1-|x|^2\right)\sin(\varphi_{10}+\varphi_S)|\mathcal{C}_{10}||S| - 4|x||S|^2\sin 2\varphi_S}{(1+|x|)^2|\mathcal{C}_{10}|^2 - 2\left(1-|x|^2\right)\cos(\varphi_{10}-\varphi_S)|\mathcal{C}_{10}||S| + 2(1+|x|^2)|S|^2} \tag{129}$$

$$\mathcal{C}_{\mu\mu}|_{\Delta=180^\circ} = \frac{2|S|\left[(1+|x|)^2|\mathcal{C}_{10}|\cos(\varphi_{10}-\varphi_S) - (1-|x|^2)|S|\right]}{(1+|x|)^2|\mathcal{C}_{10}|^2 - 2\left(1-|x|^2\right)\cos(\varphi_{10}-\varphi_S)|\mathcal{C}_{10}||S| + 2(1+|x|^2)|S|^2}. \tag{130}$$

These equations could be solved numerically to determine $|x|$, $|S|$ and φ_S, in analogy to the discussion of $\Delta = 0^\circ$.

It is interesting to have a closer look at $x = -1$, i.e. $|x| = 1$ and $\Delta = 180^\circ$. In terms of the short-distance coefficients, this case corresponds to

$$C_S = -C_S'. \tag{131}$$

Using the relations in Eqs. (63) and (64), we obtain furthermore

$$C_P = C_P', \tag{132}$$

implying

$$P = \mathcal{C}_{10}. \tag{133}$$

Using Eqs. (26) and (27), we obtain

$$|S|^2 = \frac{\left(1+y_s\right)\overline{R} - \left[1+y_s\cos(2\varphi_{10})\right]|\mathcal{C}_{10}|^2}{1-y_s\cos(2\varphi_S)}. \tag{134}$$

Special care should be paid when using Eq. (134), since the expression on the right-hand side has to be greater than or equal to zero. This feature implies the following upper bound:

$$|\mathcal{C}_{10}| \le \sqrt{\left(\frac{1+y_s}{1-y_s}\right)\overline{R}}, \tag{135}$$

where we have used that $1+y_s\cos(2\varphi_{10}) \ge 1-y_s$, with y_s given in Eq. (12). With the current experimental value of $\overline{R}$ in Eq. (28), the corresponding bound is given by

$$|\mathcal{C}_{10}| \le 0.98 \pm 0.09. \tag{136}$$

The different scenarios described in the previous sections are presented in Table 2, where we show the connection between the standard parametrization used for the short distance contributions and the SMEFT one introduced in Sec. 4.1.

5 Experimental aspects

Up to now we have not considered experimental uncertainties in the observables $\mathcal{A}_{\Delta\Gamma_s}^{\mu\mu}$, $\mathcal{S}_{\mu\mu}$ and $\mathcal{C}_{\mu\mu}$ when studying the dif-

Table 2 Summary of the scenarios described in Sect. 4.4. In all the cases we have assumed $\varphi_{10} = 0°$

Sections	SMEFT parameterization		Standard parameterization		Extra assumptions
4.4.1	$x = 0$		$C'_S = C'_P = 0$		$\lvert\mathcal{C}_{10}\rvert = 1$, $\lvert\mathcal{C}_{10}\rvert = 0.84$
	$\lvert x\rvert \to \infty$		$C_S = -C_P = 0$		
4.4.2	$\Delta = 0°$,	$\lvert x\rvert = 0.5$	$\tilde{\varphi}_S = \tilde{\varphi}'_S$,	$\lvert C_S\rvert = 2\lvert C'_S\rvert$	$\lvert\mathcal{C}_{10}\rvert = 1$
	$\Delta = 0°$,	$\lvert x\rvert = 2$	$\tilde{\varphi}_S = \tilde{\varphi}'_S$,	$\lvert C_S\rvert = 0.5\lvert C'_S\rvert$	
4.4.3	$\Delta = 180°$,	$\lvert x\rvert = 1$	$C_S = -C'_S$,	$C_P = C'_P$	

ferent scenarios. Nevertheless, we would like to demonstrate the potential for the determination of the underlying parameters at future experiments. Since the asymmetries are not independent, due to the relation in Eq. (1), it is not possible to determine all four parameters $|S|$, φ_S, $|x|$ and Δ. However, as discussed in Sect. 4.3, we expect to have a better picture of physics beyond the SM by the time the CP asymmetries of $B_s^0 \to \mu^+\mu^-$ have been measured. Therefore, we consider some of the examples discussed in Sect. 4.4, which correspond to specific values of $|x|$ or Δ. We assume uncertainties for the observables, allowing us to extract the NP parameters through fits.

Unless specified otherwise, within this section we use a future measurement of

$$\overline{R} = 0.84 \pm 0.09, \tag{137}$$

where we have assumed a relative uncertainty of 10% for $\overline{\mathcal{B}}(B_s \to \mu^+\mu^-)$, which is achievable at the LHCb upgrade [33], while keeping the current central value fixed. Notice that the relative uncertainty in our "measurement" for $\bar{R}$ in Eq. (137) leads to a 2σ tension with the SM. Thus the statistical significance will not be high enough to claim for the discovery of NP effects. The major limiting factor of the precision is the ratio f_d/f_s of the fragmentation functions of the B_d^0 and B_s^0 mesons [34], which is required for normalization purposes. To the best of our knowledge, no information about the expected precision of future measurements of $\mathcal{A}^{\mu\mu}_{\Delta\Gamma_s}$, $\mathcal{S}_{\mu\mu}$ and $\mathcal{C}_{\mu\mu}$ is available. The key question we want to address is the precision of the measurement of these observables that is required to establish in particular new (pseudo)-scalar contributions at the $5\,\sigma$ confidence level.

5.1 $x = 0$ and $|x| \to \infty$

To begin with, we evaluate the impact of experimental errors for the observables in Example (a) of Sect. 4.4.1, corresponding to a scenario where $x = 0$. An absolute uncertainty of ± 0.2 for the asymmetries leads to the following set of observables:

$$\mathcal{A}^{\mu\mu}_{\Delta\Gamma_s} = 0.58 \pm 0.20, \quad \mathcal{S}_{\mu\mu} = -0.80 \pm 0.20, \quad \mathcal{C}_{\mu\mu} = 0.16 \pm 0.20. \tag{138}$$

In such a situation, $\mathcal{S}_{\mu\mu}$ would indicate CP-violating NP effects at the 4σ level, while $\mathcal{A}^{\mu\mu}_{\Delta\Gamma_s}$ and $\mathcal{C}_{\mu\mu}$ would deviate from the SM picture at the 2σ and 1σ levels, respectively. Let us assume that the values above have been measured at a future experiment, and that there are strong reasons to consider models characterized by $x = 0$. We will now illustrate through a χ^2 fit how well we can reveal the underlying decay dynamics.

Let us first obtain the regions allowed for $|S|$ and φ_S if we only include $\overline{R}$ and $\mathcal{A}^{\mu\mu}_{\Delta\Gamma_s}$ in the statistical analysis. Thus, using the expression in Eqs. (89) and (90) with the "data" in Eqs. (137) and (138), we perform a χ^2 fit to these two observables and obtain the blue contours in the left panel of Fig. 13, which correspond to 1σ allowed regions. We indicate the input parameters used to determine our observables in Eq. (138) with the green dot. This plot allows us to establish a non-zero value for $|S|$ at the 3σ level. If we include also the "measurement" for $\mathcal{S}_{\mu\mu}$ indicated in Eq. (138), along with Eq. (91), and repeat the χ^2 fit, we can eliminate the dashed contour in the left panel and obtain the right plot of Fig. 13.

As we have pointed out in Sect. 4.4.1, there is a symmetry between $x = 0$ and $|x| \to \infty$, implying the same values of $\mathcal{A}^{\mu\mu}_{\Delta\Gamma_s}$ and $\mathcal{S}_{\mu\mu}$ for these two cases. Conversely, we could not distinguish $x = 0$ and $|x| \to \infty$ at the phenomenological level having only measurements of these observables available. Indeed, repeating the χ^2 fits assuming $|x| \to \infty$ for the same set of input observables leads to the red contours in Fig. 13. Although we use $x = 0$ as our favoured model in this illustration, it would certainly be desirable to rule out the degenerate $|x| \to \infty$ scenario. As $\mathcal{C}_{\mu\mu}$ breaks the symmetry by an overall minus sign, we could actually exclude the $|x| \to \infty$ case through experimental information on the sign on this CP asymmetry. If we add $\mathcal{C}_{\mu\mu}$ to the analysis, a solution only arises in case of the $x = 0$ scenario, thereby singling out the blue contour. We would then find

$$|S| = 0.43^{+0.07}_{-0.08}, \quad \varphi_S = (54^{+6}_{-7})°, \tag{139}$$

where $\mathcal{C}_{\mu\mu}$ has a minor impact on the numerical values themselves, apart from excluding $|x| \to \infty$. In this scenario, the assumed experimental uncertainties in Eq. (138) would allow us to establish non-zero values of $|S|$ and φ_S at the 5σ and 7σ

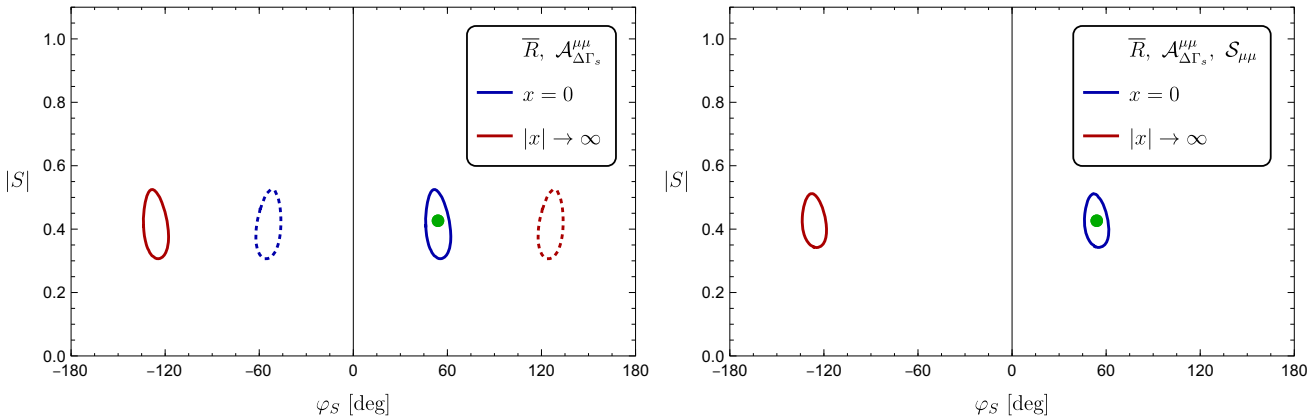

Fig. 13 Illustration of the determination of $|S|$ and φ_S from the observables in Eq. (138) for a scenario with $x = 0$, which is degenerate with $|x| \to \infty$. The contours correspond to the 1σ allowed regions obtained from χ^2 fits. In the left panel, we show the result of the fit to only $\overline{R}$ and $\mathcal{A}^{\mu\mu}_{\Delta\Gamma_s}$, while in the right panel we have also included $\mathcal{S}_{\mu\mu}$. The blue contours were obtained by assuming $x = 0$, whereas the red contours follow for $|x| \to \infty$. A measurement of the sign of $\mathcal{C}_{\mu\mu}$ would allow us to distinguish these cases, excluding the $|x| \to \infty$ scenario

levels, respectively, which would provide highly non-trivial insights into the underlying dynamics.

5.2 $\Delta = 0°$

Let us now have a closer look at another interesting scenario: $\Delta = 0°$, where C_S' and C_S have the same CP-violating phases. The expressions in Eqs. (112)–(115) form a system of three independent equations which allows us to determine $|S|$, φ_S and $|x|$. Due to the highly non-linear structure of the mathematical expressions, we cannot provide analytical solutions in general. Instead we give an example of how to solve the system through a χ^2 fit. We consider the input parameters

$$|x| = 0.5, \qquad \varphi_S = 20°, \quad |\mathcal{C}_{10}| = 1, \quad \varphi_{10} = 0°, \tag{140}$$

allowing us to determine the following solution for $|S|$, which is consistent with the current central value for $\overline{R}$ shown in Eq. (28):

$$|S| = 0.55. \tag{141}$$

If we use the previous numerical values in Eqs. (113)–(115), our observables are

$$\mathcal{A}^{\mu\mu}_{\Delta\Gamma_s} = -0.27 \pm 0.20, \quad \mathcal{S}_{\mu\mu} = 0.46 \pm 0.20, \quad \mathcal{C}_{\mu\mu} = -0.85 \pm 0.20, \tag{142}$$

where we have considered the same absolute uncertainties as in Sect. 5.1. Assuming that these observables have been measured correspondingly at a future experiment, $\mathcal{A}^{\mu\mu}_{\Delta\Gamma_s}$ would indicate NP at the 6σ level, while $\mathcal{S}_{\mu\mu}$ and $\mathcal{C}_{\mu\mu}$ would differ from the SM at the 2σ and 4σ levels, respectively. The latter observable would require a non-vanishing scalar contribution S. Performing a χ^2 fit to these quantities, we can determine the underlying decay parameters $|x|$, $|S|$ and φ_S simultaneously from the best fit point.

We start our statistical analysis by considering only $\overline{R}$, $\mathcal{A}^{\mu\mu}_{\Delta\Gamma_s}$ and $\mathcal{S}_{\mu\mu}$. In the left and right panels of Fig. 14, we show the corresponding $1\,\sigma$ confidence regions in the φ_S–$|S|$ and φ_S–$|x|$ planes, respectively. We obtain two solutions, given by the blue and red contours, as we expect based on the symmetry relations in Eq. (117). Our input parameters are indicated by the green dot. Consequently, non-zero values of $|S|$ and $|x|$ at the 4σ and 6σ levels, respectively, could then be established.

If we include also $\mathcal{C}_{\mu\mu}$ in the analysis, we can eliminate the solution corresponding to the red contours, since $\mathcal{C}_{\mu\mu}$ breaks the symmetry relation in Eq. (116) by an overall minus sign. The resulting 1σ regions are shown in Fig. 15, corresponding to the results

$$|S| = 0.55^{+0.08}_{-0.10}, \quad \varphi_S = (20^{+5}_{-5})°, \quad |x| = 0.50^{+0.07}_{-0.07}. \tag{143}$$

As a matter of fact, non-zero values of these parameters could be pinned down at the 5σ, 4σ and 7σ levels, respectively.

In general, the precision for the CP asymmetries required to determine $|S|$, φ_S and $|x|$ with a given confidence level depends on the situation in parameter space. Moreover, we may end up with an ambiguity even after including $\mathcal{C}_{\mu\mu}$ in the χ^2 fit. Nevertheless, this example nicely complements the one in Sect. 5.1 and shows the potential of the CP asymmetries to determine the (pseudo)-scalar contributions, and even to discriminate between the corresponding primed and unprimed Wilson coefficients.

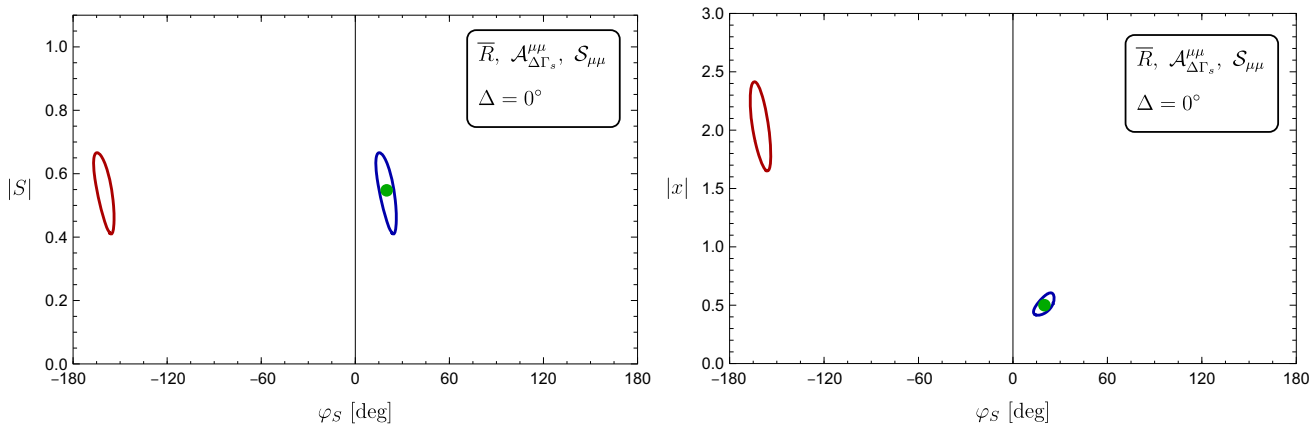

Fig. 14 Illustration of the determination of $|S|$, $|x|$ and φ_S in the scenario where we assume $\Delta = 0°$. The contours correspond to the 1σ allowed regions obtained by performing a χ^2 fit to $\overline{R}$, $\mathcal{A}^{\mu\mu}_{\Delta\Gamma_s}$ and $\mathcal{S}_{\mu\mu}$ given in Eq. (142). We obtain two solutions, indicated in blue and red, as expected from the symmetry relations in Eq. (117). The green dot marks the input parameters given in Eqs. (140) and (141)

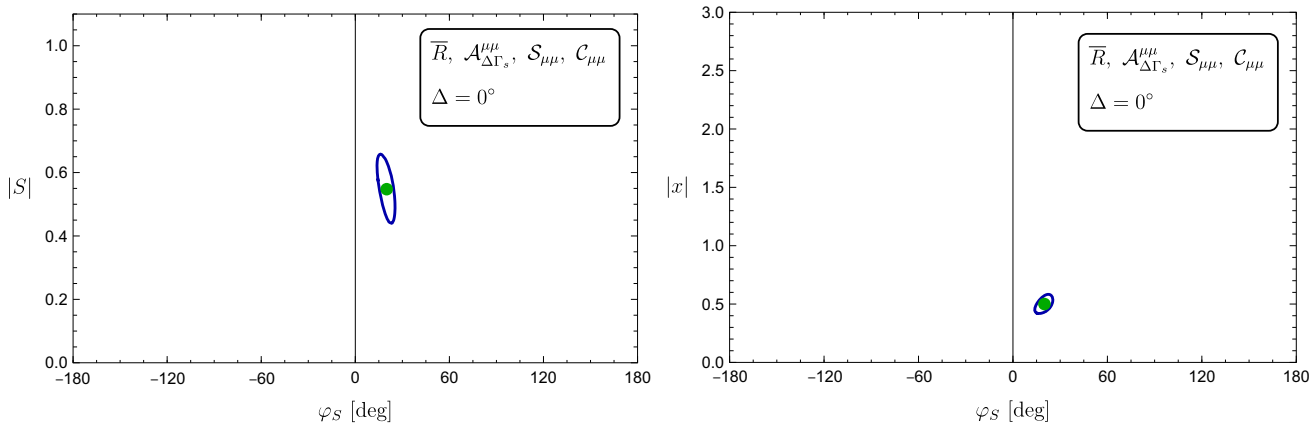

Fig. 15 Illustration of the determination of $|S|$, $|x|$ and φ_S in a scenario where we assume $\Delta = 0°$. The contours correspond to the 1σ allowed regions obtained by performing a χ^2 fit to $\overline{R}$, $\mathcal{A}^{\mu\mu}_{\Delta\Gamma_s}$, $\mathcal{S}_{\mu\mu}$ and $\mathcal{C}_{\mu\mu}$ given in Eq. (142). The green dot marks the input parameters given in Eqs. (140) and (141)

6 Conclusions and outlook

The rare decay $B_s^0 \to \mu^+\mu^-$ has been in the focus of particle physics for decades, offering one of the theoretically cleanest probes for physics beyond the SM, in particular for new (pseudo)-scalar contributions, which are still largely unconstrained. Finally, this channel could be observed by the CMS and LHCb collaborations and is now an experimentally well established process, exhibiting a branching ratio encoded in $\overline{R}$ in the ballpark of the SM. The observable $\mathcal{A}^{\mu\mu}_{\Delta\Gamma_s}$, which is accessible thanks to the decay width difference $\Delta\Gamma_s$ and requires an untagged – but time-dependent – analysis, will play an important role to shed light on possible NP contributions to $B_s^0 \to \mu^+\mu^-$. In general, these effects involve also CP-violating phases, which are usually neglected in theoretical analyses for simplicity.

In this paper, we have presented a comprehensive strategy for the future LHC upgrade(s), allowing us to reveal the presence of new sources of CP violation. The key role in this endeavour is played by the mixing-induced CP asymmetry $\mathcal{S}_{\mu\mu}$, which requires – in contrast to $\mathcal{A}^{\mu\mu}_{\Delta\Gamma_s}$ – also tagging information for the experimental analysis. Another observable, $\mathcal{C}_{\mu\mu}$, would become accessible if the helicity of the final-state muons could be determined; already sign information for this CP asymmetry would be very valuable information. These three observables do not depend on the decay constant f_{B_s} and are not affected by theoretical uncertainties.

Interestingly, the interplay of $\overline{R}$ with $\mathcal{A}^{\mu\mu}_{\Delta\Gamma_s}$ and $\mathcal{S}_{\mu\mu}$ allows us to establish new (pseudo)-scalar contributions and new sources of CP violation. In general, we can only obtain constraints as we do not have sufficient independent observables to determine the short-distance coefficients $|S|$, $|P|$ and their phases φ_S, φ_P. To obtain further insights, additional information is required. This could either be obtained by assuming specific NP models, or in a model-independent way through relations between the short-distance coefficients $C_P^{(\prime)}$, $C_S^{(\prime)}$,

which can be derived within the SMEFT approach. We have followed the latter avenue, discussing a variety of scenarios to illustrate how the corresponding parameters can be determined from the measured observables.

Since the pseudo-scalar coefficient P involves $\mathcal{C}_{10}$, we need information on this quantity. By the time precise measurements of the observables $\mathcal{A}^{\mu\mu}_{\Delta\Gamma_s}$ and $\mathcal{S}_{\mu\mu}$ are available, we expect to have a detailed picture of $\mathcal{C}_{10}$, following from analyses of semileptonic rare $B \to K^{(*)}\mu^+\mu^-$ and $B_s \to \phi\mu^+\mu^-$ decays. Current anomalies in the data for the former and $B \to K^{(*)}e^+e^-$ decays indicate NP effects in $\mathcal{C}_{10}$, which we have also considered in our explorations. It will be important to utilize CP violation in the corresponding observables in the future.

To the best of our knowledge, experimental feasibility studies for the measurement of $\mathcal{S}_{\mu\mu}$ at the LHC upgrade(s) are not yet available. Performing fits to the observables for given future scenarios, we find that an absolute precision at the 0.2 level for $\mathcal{A}^{\mu\mu}_{\Delta\Gamma_s}$ and $\mathcal{S}_{\mu\mu}$ could have a dramatic impact on our search for new (pseudo)-scalar contributions in leptonic rare B_s decays, allowing us to reveal the underlying dynamics. We urge the LHC collaborations to add studies of CP violation in rare $B^0_s \to \ell^+\ell^-$ decays to their physics agenda for the long-term future and super-high-precision era of B physics.

Acknowledgements This research has been supported by the Netherlands Foundation for Fundamental Research of Matter (FOM) programme 156, "Higgs as Probe and Portal", and by the National Organisation for Scientific Research (NWO). D.G.E. acknowledges the support through a fellowship by the Université Paris-Sud and the hospitality by Nikhef and the Vrije Universiteit Amsterdam during her visit. We would like to thank Marcel Merk for useful discussions.

Appendix

In this appendix, we collect formulae which are useful for the analysis of $B^0_s \to \mu^+\mu^-$ within the SMEFT framework introduced in Sect. 4.1. These expressions can be applied to any SMEFT scenario. In order to obtain the relevant observables in terms of the parameters $|S|$, φ_S, $|x|$ and Δ, we write Eq. (66) as

$$|P|\cos\varphi_P = |\mathcal{C}_{10}|\cos\varphi_{10} - \frac{1}{w}\left[\frac{(1-|x|^2)\cos\varphi_S - 2|x|\sin\Delta\sin\varphi_S}{1-2|x|\cos\Delta+|x|^2}\right]|S| \tag{144}$$

$$|P|\sin\varphi_P = |\mathcal{C}_{10}|\sin\varphi_{10} - \frac{1}{w}\left[\frac{(1-|x|^2)\sin\varphi_S + 2|x|\sin\Delta\cos\varphi_S}{1-2|x|\cos\Delta+|x|^2}\right]|S|, \tag{145}$$

yielding

$$\tan\varphi_P = \frac{|\mathcal{C}_{10}|\sin\varphi_{10} - \left[(1-|x|^2)\sin\varphi_S + 2|x|\sin\Delta\cos\varphi_S\right]G}{|\mathcal{C}_{10}|\cos\varphi_{10} - \left[(1-|x|^2)\cos\varphi_S - 2|x|\sin\Delta\sin\varphi_S\right]G} \tag{146}$$

with

$$G \equiv \frac{|S|}{w\left(1-2|x|\cos\Delta+|x|^2\right)}\,. \tag{147}$$

The scalar coefficient function is given as,

$$S \equiv |S|e^{i\varphi_S} = w\frac{M^2_{B_s}}{2m_\mu}\left(\frac{m_b}{m_b+m_s}\right)\left(\frac{|C_S|}{C^{\rm SM}_{10}}\right) \times\left(1-|x|e^{i\Delta}\right)e^{i\tilde{\varphi}_S} \tag{148}$$

with

$$\tan\varphi_S = \frac{(1-|x|\cos\Delta)\sin\tilde{\varphi}_S - |x|\sin\Delta\cos\tilde{\varphi}_S}{(1-|x|\cos\Delta)\cos\tilde{\varphi}_S + |x|\sin\Delta\sin\tilde{\varphi}_S}. \tag{149}$$

As we noted in Eq. (10), $C^{\rm SM}_{10}$ is negative. We may also convert φ_S into $\tilde{\varphi}_S$:

$$\begin{aligned}\cos\tilde{\varphi}_S &\propto |x|\cos(\varphi_S-\Delta) - \cos\varphi_S,\\ \sin\tilde{\varphi}_S &\propto |x|\sin(\varphi_S-\Delta) - \sin\varphi_S,\end{aligned} \tag{150}$$

which yields

$$\tan\tilde{\varphi}_S = \frac{(1-|x|\cos\Delta)\sin\varphi_S + |x|\sin\Delta\cos\varphi_S}{(1-|x|\cos\Delta)\cos\varphi_S - |x|\sin\Delta\sin\varphi_S}. \tag{151}$$

Moreover, we have

$$|C_S| = \frac{1}{w}\frac{2m_\mu}{M^2_{B_s}}\left(\frac{m_b+m_s}{m_b}\right)\frac{|C^{\rm SM}_{10}|}{\sqrt{1-2|x|\cos\Delta+|x|^2}}|S|. \tag{152}$$

The observables in Eqs. (13), and (36) and (38) require the quantities

$$\begin{aligned}|P|^2 = |\mathcal{C}_{10}|^2 &- 2\Big[(1-|x|^2)\cos(\varphi_{10}-\varphi_S)\\ &+ 2|x|\sin\Delta\sin(\varphi_{10}-\varphi_S)\Big]|\mathcal{C}_{10}|G\\ &+\left[\left(1-|x|^2\right)^2 + (2|x|\sin\Delta)^2\right]G^2,\end{aligned} \tag{153}$$

$$
\begin{aligned}
|P|^2\cos 2\varphi_P &= |P|^2\left(\cos^2\varphi_P-\sin^2\varphi_P\right)\\
&= |\mathcal{C}_{10}|^2\cos 2\varphi_{10}-2\Big[\left(1-|x|^2\right)\cos(\varphi_{10}+\varphi_S)\\
&\quad -2|x|\sin\Delta\sin(\varphi_{10}+\varphi_S)\Big]|\mathcal{C}_{10}|G\\
&\quad +\Big[\left\{\left(1-|x|^2\right)^2-(2|x|\sin\Delta)^2\right\}\cos 2\varphi_S\\
&\quad -4|x|\left(1-|x|^2\right)\sin\Delta\sin 2\varphi_s\Big]G^2, \qquad (154)\\
|P|^2\sin 2\varphi_P &= 2|P|\sin\varphi_P|P|\cos\varphi_P\\
&= |\mathcal{C}_{10}|^2\sin 2\varphi_{10}-2\Big[\left(1-|x|^2\right)\sin(\varphi_{10}+\varphi_S)\\
&\quad +2|x|\sin\Delta\cos(\varphi_{10}+\varphi_S)\Big]|\mathcal{C}_{10}|G\\
&\quad +\Big[\left\{\left(1-|x|^2\right)^2-(2|x|\sin\Delta)^2\right\}\sin 2\varphi_S\\
&\quad +4|x|\left(1-|x|^2\right)\sin\Delta\cos 2\varphi_s\Big]G^2, \qquad (155)
\end{aligned}
$$

while the CP asymmetry in Eq. (35) involves

$$
\begin{aligned}
|P||S|\cos(\varphi_P-\varphi_S) = |S|\Bigg[&|\mathcal{C}_{10}|\cos(\varphi_{10}-\varphi_S)\\
&-\left(\frac{1-|x|^2}{1-2|x|\cos\Delta+|x|^2}\right)\frac{|S|}{w}\Bigg]. \qquad (156)
\end{aligned}
$$

In view of the complexity of the resulting general expressions, we refrain from listing them for the observables r, $\mathcal{A}^{\mu\mu}_{\Delta\Gamma_s}$, $\mathcal{S}_{\mu\mu}$ and $\mathcal{C}_{\mu\mu}$. However, we have given formulae for specific examples discussed in Sect. 4.4.

References

1. C. Bobeth, M. Gorbahn, T. Hermann, M. Misiak, E. Stamou, M. Steinhauser, Phys. Rev. Lett. **112**, 101801 (2014). https://doi.org/10.1103/PhysRevLett.112.101801. arXiv:1311.0903 [hep-ph]
2. S. Aoki et al., Eur. Phys. J. C **77**(2), 112 (2017). https://doi.org/10.1140/epjc/s10052-016-4509-7. arXiv:1607.00299 [hep-lat]
3. G. Borissov, R. Fleischer, M.H. Schune, Ann. Rev. Nucl. Part. Sci. **63**, 205 (2013). https://doi.org/10.1146/annurev-nucl-102912-144527. arXiv:1303.5575 [hep-ph]
4. V. Khachatryan et al. [CMS and LHCb Collaborations], Nature **522**, 68 (2015). https://doi.org/10.1038/nature14474. arXiv:1411.4413 [hep-ex]
5. K. De Bruyn, R. Fleischer, R. Knegjens, P. Koppenburg, M. Merk, A. Pellegrino, N. Tuning, Phys. Rev. Lett. **109**, 041801 (2012). https://doi.org/10.1103/PhysRevLett.109.041801. arXiv:1204.1737 [hep-ph]
6. A.J. Buras, R. Fleischer, J. Girrbach, R. Knegjens, JHEP **1307**, 77 (2013). https://doi.org/10.1007/JHEP07(2013)077. arXiv:1303.3820 [hep-ph]
7. W. Altmannshofer, C. Niehoff, D.M. Straub, JHEP **1705**, 076 (2017). https://doi.org/10.1007/JHEP05(2017)076. arXiv:1702.05498 [hep-ph]
8. R. Fleischer, R. Jaarsma, G. Tetlalmatzi-Xolocotzi, JHEP **1705**, 156 (2017). https://doi.org/10.1007/JHEP05(2017)156. arXiv:1703.10160 [hep-ph]
9. R. Aaij et al. [LHCb Collaboration], Phys. Rev. Lett. **118**(19), 191801 (2017). https://doi.org/10.1103/PhysRevLett.118.191801. arXiv:1703.05747 [hep-ex]
10. G. D'Ambrosio, G.F. Giudice, G. Isidori, A. Strumia, Nucl. Phys. B **645**, 155 (2002). https://doi.org/10.1016/S0550-3213(02)00836-2. arXiv:hep-ph/0207036
11. G. Buchalla, A.J. Buras, M.E. Lautenbacher, Rev. Mod. Phys. **68**, 1125 (1996). https://doi.org/10.1103/RevModPhys.68.1125. arXiv:hep-ph/9512380
12. I. Dunietz, R. Fleischer, U. Nierste, Phys. Rev. D **63**, 114015 (2001). https://doi.org/10.1103/PhysRevD.63.114015. arXiv:hep-ph/0012219
13. K. De Bruyn, R. Fleischer, R. Knegjens, P. Koppenburg, M. Merk, N. Tuning, Phys. Rev. D **86**, 014027 (2012). https://doi.org/10.1103/PhysRevD.86.014027. arXiv:1204.1735 [hep-ph]
14. Y. Amhis et al. [Heavy Flavor Averaging Group]. arXiv:1612.07233 [hep-ex] and online update at http://www.slac.stanford.edu/xorg/hfag/
15. K. De Bruyn, R. Fleischer, JHEP **1503**, 145 (2015). https://doi.org/10.1007/JHEP03(2015)145. arXiv:1412.6834 [hep-ph]
16. J. Charles et al. Phys. Rev. D **91**(7), 073007 (2015). https://doi.org/10.1103/PhysRevD.91.073007. arXiv:1501.05013 [hep-ph] (**for updates, see** http://ckmfitter.in2p3.fr]
17. S. Chatrchyan et al. [CMS Collaboration], Phys. Rev. Lett. **111**, 101804 (2013). https://doi.org/10.1103/PhysRevLett.111.101804. arXiv:1307.5025 [hep-ex]
18. C. Patrignani et al. [Particle Data Group], Chin. Phys. C **40**(10), 100001 (2016). https://doi.org/10.1088/1674-1137/40/10/100001
19. M. Aaboud et al. [ATLAS Collaboration], Eur. Phys. J. C **76**(9), 513 (2016). https://doi.org/10.1140/epjc/s10052-016-4338-8. arXiv:1604.04263 [hep-ex]
20. M. Beneke, C. Bobeth, R. Szafron. arXiv:1708.09152 [hep-ph]
21. C.S. Huang, W. Liao, Phys. Lett. B **525**, 107 (2002). https://doi.org/10.1016/S0370-2693(01)01427-7. arXiv:hep-ph/0011089
22. A. Dedes, A. Pilaftsis, Phys. Rev. D **67**, 015012 (2003). https://doi.org/10.1103/PhysRevD.67.015012. arXiv:hep-ph/0209306
23. P.H. Chankowski, J. Kalinowski, Z. Was, M. Worek, Nucl. Phys. B **713**, 555 (2005). https://doi.org/10.1016/j.nuclphysb.2005.02.010. arXiv:hep-ph/0412253
24. W. Buchmüller, D. Wyler, Nucl. Phys. B **268**, 621 (1986). https://doi.org/10.1016/0550-3213(86)90262-2
25. B. Grzadkowski, M. Iskrzynski, M. Misiak, J. Rosiek, JHEP **1010**, 085 (2010). https://doi.org/10.1007/JHEP10(2010)085. arXiv:1008.4884 [hep-ph]
26. R. Alonso, B. Grinstein, J. Martin, Camalich, Phys. Rev. Lett. **113**, 241802 (2014). https://doi.org/10.1103/PhysRevLett.113.241802. arXiv:1407.7044 [hep-ph]
27. F. Beaujean, C. Bobeth, S. Jahn, Eur. Phys. J. C **75**(9), 456 (2015). https://doi.org/10.1140/epjc/s10052-015-3676-2. arXiv:1508.01526 [hep-ph]
28. W. Altmannshofer, C. Niehoff, P. Stangl, D.M. Straub, Eur. Phys. J. C **77**(6), 377 (2017). https://doi.org/10.1140/epjc/s10052-017-4952-0. arXiv:1703.09189 [hep-ph]
29. W. Altmannshofer, D.M. Straub, Eur. Phys. J. C **75**(8), 382 (2015). https://doi.org/10.1140/epjc/s10052-015-3602-7. arXiv:1411.3161 [hep-ph]
30. C. Bobeth, G. Hiller, D. van Dyk, JHEP **1107**, 067 (2011). https://doi.org/10.1007/JHEP07(2011)067. arXiv:1105.0376 [hep-ph]
31. A.K. Alok, B. Bhattacharya, D. Kumar, J. Kumar, D. London, S.U. Sankar, Phys. Rev. D **96**(1), 015034 (2017). https://doi.org/10.1103/PhysRevD.96.015034. arXiv:1703.09247 [hep-ph]
32. C. Bobeth, A.J. Buras, A. Celis, M. Jung, JHEP **1704**, 079 (2017). https://doi.org/10.1007/JHEP04(2017)079. arXiv:1609.04783 [hep-ph]

33. R. Aaij et al. [LHCb Collaboration], Eur. Phys. J. C **73**, 2373 (2013). https://doi.org/10.1140/epjc/s10052-013-2373-2. arXiv:1208.3355 [hep-ex]

34. R. Fleischer, N. Serra, N. Tuning, Phys. Rev. D **82**, 034038 (2010). https://doi.org/10.1103/PhysRevD.82.034038. arXiv:1004.3982 [hep-ph]